

1 **Inference of photosynthetic capacity parameters from Chlorophyll a**  
2 **Fluorescence is affected by redox state of PSII reaction centers**

3 Jimei Han<sup>1\*</sup>, Lianhong Gu<sup>2</sup>, Jiaming Wen<sup>1</sup>, Ying Sun<sup>1\*</sup>

4 <sup>1</sup>School of Integrative Plant Science, Soil and Crop Science Section, Cornell University, Ithaca,  
5 NY, USA

6 <sup>2</sup>Environmental Sciences Division and Climate Change Science Institute, Oak Ridge National  
7 Laboratory, Oak Ridge, Tennessee, USA

8 \*Corresponding to: [jh2757@cornell.edu](mailto:jh2757@cornell.edu) (J. Han), [ys776@cornell.edu](mailto:ys776@cornell.edu) (Y. Sun)

9

10 This manuscript has been co-authored by UT-Battelle, LLC under Contract No. DE-AC05-00OR22725 with the U.S.  
11 Department of Energy. The United States Government retains and the publisher, by accepting the article for  
12 publication, acknowledges that the United States Government retains a non-exclusive, paid-up, irrevocable, worldwide  
13 license to publish or reproduce the published form of this manuscript, or allow others to do so, for United States  
14 Government purposes. The Department of Energy will provide public access to these results of federally sponsored  
15 research in accordance with the DOE Public Access Plan (<http://energy.gov/downloads/doe-public-access-plan>).

16

17

## 18 **Abstract**

19 Solar-Induced chlorophyll Fluorescence (SIF) has been used to infer photosynthetic capacity  
20 parameters (*e.g.*, the maximum carboxylation rate  $V_{\text{cmax}}$ , and the maximum electron transport rate  
21  $J_{\text{max}}$ ). However, the precise mechanism and practical utility of such approach under dynamic  
22 environments remain unclear. We used the balance between the light and carbon reactions to derive  
23 theoretical equations relating chlorophyll *a* fluorescence (ChlF) emission and photosynthetic  
24 capacity parameters, and formulated testable hypotheses regarding the dynamic relationships  
25 between the true total ChlF emitted from PSII ( $SIF_{\text{PSII}}$ ) and  $V_{\text{cmax}}$  and  $J_{\text{max}}$ . We employed  
26 concurrent measurements of gas exchanges and ChlF parameters for 15 species from six biomes  
27 to test the formulated hypotheses across species, temperatures, and limitation state of  
28 carboxylation. Our results revealed that  $SIF_{\text{PSII}}$  alone is incapable of informing the variations in  
29  $V_{\text{cmax}}$  and  $J_{\text{max}}$  across species, even when  $SIF_{\text{PSII}}$  is determined under the same environmental  
30 conditions. In contrast, the product of  $SIF_{\text{PSII}}$  and the fraction of open PSII reactions  $q_L$ , which  
31 indicates the redox state of PSII, is a strong predictor of both  $V_{\text{cmax}}$  and  $J_{\text{max}}$ , although their precise  
32 relationships vary somewhat with environmental conditions. Our findings suggest the redox state  
33 of PSII strongly influences the relationship between  $SIF_{\text{PSII}}$  and  $V_{\text{cmax}}$  and  $J_{\text{max}}$ .

34 **Key words:** Limitation state of carboxylation; photosynthetic capacity; redox state of PSII  
35 reaction centers; Solar-Induced chlorophyll Fluorescence (SIF)

36 **Summary Statement:** Our theoretical and measurement results revealed that the fraction of open  
37 PSII reaction centers  $q_L$ , which indicates the redox state of PSII plays an important role when  
38 chlorophyll *a* fluorescence is used to infer  $V_{\text{cmax}25}$  and  $J_{\text{max}25}$ . The limitation state of carboxylation

39 must be considered if observed chlorophyll *a* fluorescence is utilized to infer  $V_{\text{cmax}25}$  (or  $J_{\text{max}25}$ )  
40 under dynamic environmental conditions.

41

## 42 **Introduction**

43 Photosynthetic capacity, characterized by the maximum carboxylation rate ( $V_{\text{cmax}}$ ) of RuBisCO  
44 and the maximum electron transport rate ( $J_{\text{max}}$ ), is prime leaf trait that determine the maximum  
45 photosynthetic rate and its response to environmental changes (Wullschleger, 1993; Walker *et al.*,  
46 2014; Wright *et al.*, 2004).  $V_{\text{cmax}}$  is determined by the amount and kinetics of the active RuBisCO  
47 enzyme (ribulose 1,5-bisphosphate carboxylase/oxygenase), the key enzyme for CO<sub>2</sub> fixation  
48 during carbon reactions (Cooper, 2000; Yoshikawa, 2013; Detto & Xu, 2020). Under high light  
49 conditions, photosynthetic carboxylation is often RuBisCO limited at the current CO<sub>2</sub> level.  $J_{\text{max}}$   
50 is a key determinant of the potential electron transport rate ( $J_p$ ), which becomes the actual electron  
51 transport rate ( $J_a$ ) when photosynthetic carboxylation is limited by the Ribulose 1,5-bisphosphate  
52 (RuBP) regeneration (Gu *et al.*, 2019), often under low light conditions at the current CO<sub>2</sub>. Timely  
53 and accurate estimation of these photosynthetic capacity parameters is of vital importance for  
54 reliable prediction of large-scale carbon cycle dynamics and feedbacks to climate change using  
55 terrestrial biosphere models (TBMs) (Walker *et al.*, 2014; Rogers *et al.*, 2017) and for field-scale  
56 high-throughput crop phenotyping (Meacham-Hensold *et al.*, 2019; Fu *et al.*, 2021). From the  
57 perspective of carbon cycle modeling, TBMs (usually coupled with the Intergovernmental Panel  
58 on Climate Change IPCC global climate models) have almost exclusively adopted the Farquhar–  
59 von Caemmerer–Berry (FvCB) biochemical model (Farquhar *et al.*, 1980; von Caemmerer &  
60 Farquhar, 1981; von Caemmerer, 2020; Sharkey, 1985), which requires  $V_{\text{cmax}}$  and  $J_{\text{max}}$  as key  
61 parameters for photosynthesis calculation. Uncertainties in these parameters constitute the major  
62 sources of prediction error in the simulated photosynthesis (Bonan *et al.*, 2011; Walker *et al.*, 2014,  
63 2020; Rogers *et al.*, 2017). Their uncertainties come primarily from their huge variability within  
64 and across biomes and dependencies on leaf nitrogen/phosphorus, chlorophyll content, age, and

65 environmental conditions (Field & Mooney, 1986; Xu & Baldocchi, 2013; Monsoon & Baldocchi,  
66 2014; Walker *et al.*, 2014; Croft *et al.*, 2017; Detto & Xu, 2020; Kattge *et al.*, 2020). From the  
67 plant breeding perspective towards improving crop yields, increasing the carboxylation capacity  
68 of RuBisCO and optimizing electron transport chain are considered as promising genetic  
69 modification targets (South *et al.*, 2019; Simkin *et al.*, 2015, 2019; Bailey-Serres *et al.*, 2019).  
70 Rapid high-throughput screening of  $V_{\text{cmax}}$  and  $J_{\text{max}}$  at the field scale will greatly accelerate the  
71 efficiency of selecting crop cultivars with enhanced photosynthesis (Fu *et al.*, 2019, 2021).

72 Remote sensing observations, from satellite, airborne, to ground platforms, have been  
73 employed to infer these photosynthetic capacity parameters, with spatially and/or temporally  
74 resolved details (Croft *et al.*, 2017; Zhang *et al.*, 2014; Serbin *et al.*, 2015; Camino *et al.*, 2019;  
75 Meacham-Hensold *et al.*, 2019; Fu *et al.*, 2019, 2021; Yendrek *et al.*, 2017). Such approaches are  
76 advantageous over the traditional labor-intensive (though considered as the ground truth) leaf gas  
77 exchange measurements (Zhang *et al.*, 2014; Fu *et al.*, 2021). Majority of these remote sensing  
78 efforts have been focusing on utilizing multi- or hyper-spectral reflectance from visible, near  
79 infrared, to shortwave infrared bands. Recently, Solar-Induced chlorophyll Fluorescence (SIF)  
80 emerges as a promising remote sensing tool to infer  $V_{\text{cmax}}$  and/or  $J_{\text{max}}$  (Zhang *et al.*, 2014; Camino  
81 *et al.*, 2019; Fu *et al.*, 2021). Such promise is driven by the combination of 1) the theoretical  
82 grounds established since 1980s that chlorophyll a fluorescence (ChlF) is functionally linked to  
83 electron transport for photosynthetic activities at the molecular level (Genty *et al.*, 1989;  
84 Papageorgiou & Govindjee, 2004) and 2) the rapidly growing observing capability from satellite,  
85 airborne, to ground platforms (Frankenberg *et al.*, 2011; Joiner *et al.*, 2013; Guanter *et al.*, 2012;  
86 Mohammed *et al.*, 2019). However, mixed results have been obtained so far with respect to the  
87 relationships between SIF (or quantum yield of SIF) and  $V_{\text{cmax}}$  (or  $J_{\text{max}}$ ). For example, Zhang *et al.*

88 (2014, 2018) and Camino *et al.* (2019) reported positive SIF- $V_{\text{cmax}}$  relationships using ensemble  
89 simulations of SCOPE (Soil Canopy Observation Photosynthesis Energy, van der Tol *et al.*, 2009,  
90 2014). In contrast, Vilfan *et al.* (2019) demonstrated that SIF cannot track the variability of  $V_{\text{cmax}}$   
91 across leaves by combining leaf reflectance and transmittance in SCOPE although the magnitude  
92 of  $V_{\text{cmax}}$  can be estimated with this approach. Fu *et al.* (2021) reported negative relationships  
93 between  $J_{\text{max}}$  (and  $V_{\text{cmax}}$ ) and the quantum yield of SIF ( $\Phi_{\text{SIF}}$ ) across a variety of tobacco cultivars.  
94 Also, Koffi *et al.* (2015) showed weak sensitivity of SIF to  $V_{\text{cmax}}$  even under high light conditions  
95 (usually when carboxylation is RuBisCO limited). These conflicting findings in previous reports  
96 have yet to be reconciled.

97         Conceptually, there is a fundamental mismatch in directly relating  $V_{\text{cmax}}$  and  $J_{\text{max}}$  to SIF.  
98 The standardized  $V_{\text{cmax}}$  and  $J_{\text{max}}$  (*i.e.*,  $V_{\text{cmax}25}$  and  $J_{\text{max}25}$  at the reference temperature of 25 °C with  
99 no stress) characterize the intrinsic photosynthetic capacity of the carbon and light reactions,  
100 respectively. They are supposed to be parameters that do not depend on instantaneous changes in  
101 light levels although changes at longer time scales are possible. To the contrary, SIF can only be  
102 emitted during the light reactions and vary rapidly with the fluctuating lights in natural  
103 environment. Thus, for any SIF -  $V_{\text{cmax}}$  (or  $J_{\text{max}}$ ) relationship to be meaningful, some sort of  
104 standardization (*i.e.*, stratification to certain biotic or/and abiotic conditions) must be done for SIF.  
105 So far, no studies have examined the best way to standardize SIF for  $V_{\text{cmax}}/J_{\text{max}}$  characterization or  
106 how SIF -  $V_{\text{cmax}}$  (or  $J_{\text{max}}$ ) relationships may change under varying light intensities. Further, even  
107 with the SIF standardized in one way or the other, it is not immediately clear whether the  
108 standardized SIF -  $V_{\text{cmax}}$  (or  $J_{\text{max}}$ ) relationships should be sufficiently invariant to possess at least  
109 some predictive power.

110 This study aims to 1) understand the cause of the discrepancies among existing studies and  
111 to 2) develop a mechanistic solution for using SIF observations to infer photosynthetic capacity  
112 parameters across species in dynamic environments. We ground our study on the firmly  
113 established knowledges of the light and carbon reactions and the balance between the supply and  
114 demand of ATP and NADPH. Specifically, we first sought to establish the theoretical basis that  
115 links the true total ChlF emitted from PSII (denoted as  $SIF_{PSII}$ ) and photosynthetic capacity  
116 parameters by balancing the actual electron transport rate  $J_a$  derived by a mechanistic light reaction  
117 model (MLR-SIF, Gu *et al.*, 2019) and that derived by the Farquhar-von Caemmerer-Berry (FvCB)  
118 biochemical model (Farquhar *et al.*, 1980).  $SIF_{PSII}$  refers to the ChlF prior to signal attenuation due  
119 to leaf scattering/reabsorption, which in principle should be utilized to establish the mechanistic  
120 relationship with photosynthetic capacity parameters. Our rationale is that the foundation of  
121 remotely sensed SIF (*i.e.*, at-sensor SIF) for estimating photosynthetic capacity parameters can  
122 only be established once a solid theoretical understanding of fundamental mechanisms that govern  
123 the relationships between  $SIF_{PSII}$  and photosynthetic capacity parameters is built. We then used the  
124 established theoretical basis to formulate testable hypotheses regarding the  $SIF_{PSII} - V_{cmax} (J_{max})$   
125 relationships across species in dynamic environments. Finally, we utilized concurrent  
126 measurements of leaf-level gas exchanges and ChlF parameters of 15 species from six major plant  
127 functional types (PFTs) of the globe to test the theoretically formulated hypotheses. Once these  
128 steps were completed, we sought to answer the following questions:

- 129 - Are there unique, predictive  $SIF_{PSII} - V_{cmax} / J_{max}$  relationships across species and  
130 environmental conditions?
- 131 - If not, what factors affect  $SIF_{PSII} - V_{cmax} / J_{max}$  relationships?
- 132 - How can  $SIF_{PSII}$  be used to infer  $V_{cmax}$  and  $J_{max}$  across species in dynamic environments?

## 133 **Materials and Methods**

### 134 **Theoretical relationships of $V_{\text{cmax}}$ and $J_{\text{max}}$ with $SIF_{\text{PSII}}$ based on the balance between the** 135 **light and carbon reactions**

136 Plants have evolved sophisticated mechanisms to ensure that the supply of ATP and NADPH at  
137 the end of light reactions balances their demand in the carbon reactions (Rochaix, 2011; Joliot,  
138 2011; Kramer & Evans, 2011). This forms the theoretical basis of our derivation of the mechanistic  
139 relationships of  $V_{\text{cmax}}$  and  $J_{\text{max}}$  with  $SIF_{\text{PSII}}$  under varying environmental conditions via the actual  
140 electron transport rate  $J_a$ . From the perspective of light reactions, we used the mechanistic light  
141 reaction model (MLR-SIF) developed by Gu *et al.* (2019) for calculating  $J_a$  with  $SIF_{\text{PSII}}$  together  
142 with the fraction of open PSII reactions ( $q_L$ ) as input (eqn 1).

$$143 \quad J_a = \frac{\Phi_{PSII\text{max}} \cdot (1 + k_{DF})}{1 - \Phi_{PSII\text{max}}} \times q_L \times SIF_{PSII} \quad (\text{eqn 1})$$

144 where  $q_L$  denotes the fraction of open PSII reactions under the assumption of lake model for  
145 photosynthetic unit connectivity, and  $\Phi_{PSII\text{max}}$  the maximum photochemical yield of the dark-  
146 adapted leaves.  $K_{DF} = k_D/k_F$ , with  $k_D$  and  $k_F$  representing the rate constants of constitutive thermal  
147 dissipation and fluorescence, respectively. At the present, there are uncertainties regarding the  
148 value of  $k_D$  and  $k_F$  and therefore  $k_{DF}$ .

149 The MLR-SIF model consists of a set of fundamental equations derived from first  
150 principles that govern the fate of absorbed photons and relationships among different de-excitation  
151 pathways. At their core, these light reaction equations embody the law of conservation of energy  
152 in photosystems and are thus universal. Their exact formulation, however, depends on the

153 connectivity of photosynthetic units, which consist of coupled reaction centers and antenna  
 154 pigments. Here we used the lake model (Kramer *et al.*, 2004), which assumes that reaction centers  
 155 are embedded in a network (lake) of antenna pigments such that all photosynthetic units are  
 156 interconnected and freely share excitations. Such assumption is considered to be highly accurate  
 157 for higher plants. Detailed derivation of eqn 1 can be found in Gu *et al.* (2019).

158 From the perspective of carbon reactions, we used the classical FvCB model to link  $J_a$  with  
 159 gross photosynthetic rate  $A_g$  in  $C_3$  plant species (Farquhar *et al.*, 1980):

$$160 \quad J_a = A_g \times \frac{4C_i + 8\Gamma^*}{C_i - \Gamma^*}$$

161 (eqn 2)

162 Note this equation holds regardless of carboxylation limitation state because  $J_a$  is the actual, rather  
 163 than potential, electron transport rate.  $A_g$  (calculated with eqn 3) is essentially the sum of net  
 164 photosynthetic rate and day respiration. Eqn 2 assumes NADPH supply is limiting. If ATP is  
 165 limiting, the factor 8 on the right-hand side of eqn 2 should be replaced by the factor 9.33 (Yin *et*  
 166 *al.*, 2021). Here we did not include TPU-limited carboxylation, as this paper only concerns  $V_{cmax}$   
 167 and  $J_{max}$ .

$$168 \quad A_g = \min \{A_c, A_j\} \tag{eqn 3a}$$

$$169 \quad A_c = \frac{V_{cmax} \cdot (C_i - \Gamma^*)}{C_i + K_{co}} \tag{eqn 3b}$$

$$170 \quad A_j = \frac{J_p}{4} \times \frac{C_i - \Gamma^*}{C_i + 2\Gamma^*} \tag{eqn 3c}$$

$$J_p = \frac{\sigma \cdot PAR + J_{max} - \sqrt{(\sigma \cdot PAR + J_{max})^2 - 4\theta \cdot \sigma \cdot PAR \cdot J_{max}}}{2\theta}$$

(eqn 3d)

Here  $\Gamma^*$  and  $C_i$  denote the  $\text{CO}_2$  compensation point in the absence of mitochondrial respiration and intercellular  $\text{CO}_2$  concentration, respectively.  $K_{co}$  is a composite parameter for Michaelis-Menten constants for RuBP carboxylation and oxygenation.  $\theta$  is an empirical curvature parameter and was fixed at 0.9 (Medlyn *et al.*, 2002).  $\sigma$  is the product of  $\Phi_{PSII_{max}}$ , leaf light absorptance and fraction of absorbed photons allocated to PSII.  $\sigma$  was set to 0.3 (Long *et al.*, 1993). The values of  $\theta$  and  $\sigma$  have only a slight effect on the estimated value of  $J_{max}$  (Medlyn *et al.*, 2002).  $J_p$  is the potential electron transport rate which equals  $J_a$ , only under the RuBP regeneration limited carboxylation.

Next, by equating the light reaction-based (MLR-SIF, eqn 1) and carbon reaction-based  $J_a$  (FvCB, eqn 2-3), we can derive explicit relationships between  $SIF_{PSII}$  and  $V_{cmax}$  (and  $J_{max}$ ) (details in Notes S1). Specifically, under the Rubisco-limited state, we set  $A_g = A_c$ ; then combining eqn 2 and 3b leads to:

$$\frac{V_{cmax} \cdot (C_i - \Gamma^*)}{C_i + K_{co}} = \frac{(C_i - \Gamma^*)}{4C_i + 8\Gamma^*} \times J_a \quad (\text{eqn 4})$$

4)

Inserting eqn 1 to eqn 4 results in:

$$V_{cmax} = \frac{C_i + K_{co}}{(4C_i + 8\Gamma^*)} \times \frac{\Phi_{PSII_{max}}}{1 - \Phi_{PSII_{max}}} \times (1 + k_{DF}) \times q_L \times SIF_{PSII}. \quad (\text{eqn 5})$$

Under the RuBP regeneration limited state, the potential electron transport rate becomes the actual rate, *i.e.*,  $J_p = J_a$ , then equating eqn 1 and eqn 3d leads to

$$190 \quad J_{max} = \frac{\theta \cdot \frac{q_L \cdot SIF_{PSII} \cdot (1 + k_{DF})}{\sigma \cdot PAR} - \frac{1 - \Phi_{PSII_{max}}}{\Phi_{PSII_{max}}}}{\frac{q_L \cdot SIF_{PSII} \cdot (1 + k_{DF})}{\sigma \cdot PAR} - \frac{1 - \Phi_{PSII_{max}}}{\Phi_{PSII_{max}}}} \times \frac{\Phi_{PSII_{max}}}{1 - \Phi_{PSII_{max}}} \times (1 + k_{DF}) \times q_L \times SIF_{PSII} \quad (\text{eqn 6})$$

191 To obtain  $V_{c_{max25}}$  and  $J_{max25}$ , *i.e.*,  $V_{c_{max}}$  and  $J_{max}$  values at the 25 °C reference temperature,  
 192 we invoked the temperature response function  $f_v(T)$  and  $f_j(T)$  respectively (eqn 7a, 7b). We adopted  
 193 Arrhenius function (Arrhenius, 1915) for  $f_v(T)$  and the peaked function (Johnson *et al.*, 1942) for  
 194  $f_j(T)$  according to Medlyn *et al.* (2002).

$$195 \quad V_{c_{max}} = V_{c_{max25}} f_v(T) \quad (\text{eqn 7a})$$

$$196 \quad J_{max} = J_{max25} f_j(T) \quad (\text{eqn 7b})$$

197 where T represents the leaf temperature.

198 This leads to:

$$199 \quad V_{c_{max25}} = \frac{1}{f_v(T)} \times \frac{C_i + K_{co}}{(4C_i + 8\Gamma^*)} \times \frac{\Phi_{PSII_{max}}}{1 - \Phi_{PSII_{max}}} \times (1 + k_{DF}) \times q_L \times SIF_{PSII} \quad \text{Rubisco-limited} \quad (\text{eqn 8})$$

$$200 \quad J_{max25} = \frac{1}{f_j(T)} \times \frac{\theta \cdot \frac{q_L \cdot SIF_{PSII} \cdot (1 + k_{DF})}{\sigma \cdot PAR} - \frac{1 - \Phi_{PSII_{max}}}{\Phi_{PSII_{max}}}}{\left( \frac{q_L \cdot SIF_{PSII} \cdot (1 + k_{DF})}{\sigma \cdot PAR} - \frac{1 - \Phi_{PSII_{max}}}{\Phi_{PSII_{max}}} \right)} \times \frac{\Phi_{PSII_{max}}}{1 - \Phi_{PSII_{max}}} \times (1 + k_{DF}) \times q_L \times SIF_{PSII}$$

$$201 \quad \text{RuBP regeneration-limited} \quad (\text{eqn 9})$$

202 Eqn 5-6 and 8-9 lay the foundation for interpreting and modeling the dynamic relationship between  
 203  $SIF_{PSII}$  and photosynthetic capacity parameters under changing environmental conditions. Note  
 204 that under Rubisco-limited state, only the functional relationship of  $V_{c_{max}}$  with  $SIF_{PSII}$  was derived;  
 205 but a similar relationship is expected for  $J_{max}$  with  $SIF_{PSII}$ , as it has been well established that  $V_{c_{max}}$   
 206 and  $J_{max}$  are highly correlated across a broad range of plant biomes (Wullschleger, 1993; Walker  
 207 *et al.*, 2014). The same argument holds true for  $V_{c_{max}}$  and  $J_{max}$  under the RuBP regeneration limited

208 state. Also, we did not consider the TPU-limited carboxylation state here, as this study focuses on  
209  $V_{\text{cmax}}$  and  $J_{\text{max}}$  only; but the relationship between TPU and  $SIF_{\text{PSII}}$  can be similarly derived  
210 following the same procedure above.

211 From eqn 5 (and 8), it is immediately clear that, under Rubisco-limitation state, the  
212 relationship of  $SIF_{\text{PSII}}$  with  $V_{\text{cmax}}$  (and by extension with  $J_{\text{max}}$ ) depends on environmental conditions,  
213 because  $q_L$ ,  $C_i$ ,  $K_{\text{co}}$ , and  $\Gamma^*$  all vary with environmental conditions (*i.e.*, PAR and/or temperature).  
214 Under RuBP regeneration limitation stage in eqn 6 (and 9), the relationship of  $SIF_{\text{PSII}}$  with  $J_{\text{max}}$   
215 (and also by extension with  $V_{\text{cmax}}$ ) depends on  $q_L$  and PAR, which are highly dynamic with  
216 environmental changes. Therefore, we hypothesize the following:

- 217 - **Hypothesis I:** There is no unique relationship between  $V_{\text{cmax}25}$  (and  $J_{\text{max}25}$ ) and  $SIF_{\text{PSII}}$ .
- 218 - **Hypothesis II:**  $V_{\text{cmax}25}$  and  $J_{\text{max}25}$  are positively correlated with the product of  $q_L$  and  
219  $SIF_{\text{PSII}}$ , *i.e.*,  $SIF_{\text{PSII}} \times q_L$  (measured at the same environmental conditions).

220 When Rubisco limits carboxylation (eqn 8),  $\frac{1}{f_V(T)} \times \frac{C_i + K_{\text{co}}}{(4C_i + 8\Gamma^*)}$  should regulate the strength of the  
221 relationship between  $V_{\text{cmax}25}$  ( $J_{\text{max}25}$ ) and  $SIF_{\text{PSII}} \times q_L$ . As remote sensing SIF-based  $V_{\text{cmax}}/J_{\text{max}}$   
222 inference applies only to the ambient  $\text{CO}_2$  ( $C_a$ ), the variation in  $\frac{C_i + K_{\text{co}}}{4C_i + 8\Gamma^*}$  should be mainly due to  
223 variations in temperature if the  $C_i/C_a$  ratio is assumed to be constant. The relationship of  $V_{\text{cmax}25}$   
224 and  $J_{\text{max}25}$  with  $SIF_{\text{PSII}} \times q_L$  will be affected by the joint temperature dependence of  $\frac{C_i + K_{\text{co}}}{4C_i + 8\Gamma^*}$  and  $f_V$   
225 ( $T$ ). This motivates the third hypothesis:

- 226 - **Hypothesis III:** Under the Rubisco limitation, temperature variations increase the  
227 variability of the relationship of  $V_{\text{cmax}25}$  and  $J_{\text{max}25}$  with  $SIF_{\text{PSII}} \times q_L$ .

228 When RuBP regeneration limits carboxylation, eqn 9 reveals that  $V_{\text{cmax}}$  or  $J_{\text{max}}$  is not simply

229 linearly related to  $SIF_{\text{PSII}} \times q_L$ . The term  $\left(\frac{SIF_{\text{PSII}}}{\sigma \cdot PAR}\right)$  in the slope  $\left(\frac{\theta \cdot \frac{q_L \cdot SIF_{\text{PSII}} \cdot (1 + k_{DF})}{\sigma \cdot PAR} - \frac{1 - \Phi_{\text{PSIImax}}}{\Phi_{\text{PSIImax}}}}{\left(\frac{q_L \cdot SIF_{\text{PSII}} \cdot (1 + k_{DF})}{\sigma \cdot PAR} - \frac{1 - \Phi_{\text{PSIImax}}}{\Phi_{\text{PSIImax}}}\right)}\right)$

230 approximately equals to  $\Phi_{\text{SIF}}$  and has been shown to be relatively muted to PAR variations (Gu *et*

231 *al.*, 2019), but  $q_L$  is very sensitive to instantaneous variations in the environment factors (*e.g.*,

232 PAR, water stress, besides temperature). This reasoning leads to the fourth hypothesis:

233 - **Hypothesis IV:**  $V_{\text{cmax}25}$  and  $J_{\text{max}25}$  have stronger linear relationships with  $SIF_{\text{PSII}} \times q_L$

234 under Rubisco-limited than under RuBP regeneration-limited carboxylation state.

235 Testing these hypotheses with the concurrent measurements of leaf-level gas exchanges and ChlF

236 parameters at the leaf level is essential to better understanding how  $SIF_{\text{PSII}}$  should be used to infer

237 photosynthetic capacity parameters.

238

## 239 **Study sites and plant species**

240 To test the hypotheses inferred from theory above, we used measurements conducted at the Oak  
241 Ridge National Laboratory (ORNL), Oak Ridge, TN, U.S. (35°54'N; 84°20'W) from July to  
242 October in 2017, and Cornell Botanic Gardens (CBG), Ithaca, NY, U.S. (42°26'N; 76°28'W) from  
243 June to August in 2020. We collected concurrent measurements of leaf gas exchanges and ChlF  
244 parameters for 15 plant species (Table 1) from six major PFTs. At CBG, the average annual  
245 maximum and minimum temperatures are 13.61 °C and 2.64 °C, respectively and the average  
246 annual precipitation is 789 mm. The measured species cover boreal broadleaf deciduous trees  
247 (BDT Boreal), temperate broadleaf deciduous shrubs (BDS Temperate), temperate broadleaf  
248 deciduous trees (BDT Temperate), and C<sub>3</sub> Grass (C3G). Measurements at ORNL were made for  
249 two-year-old bare-root tree saplings and cotton grown in walk-in growth chambers. The tree  
250 saplings were from species that are representative of temperate broadleaf deciduous trees (BDT-  
251 Temperate) and boreal needle evergreen trees (NET-Boreal). They were planted into 6.2 L plastic  
252 pots filled with standard potting mix (Sungro, Canada), and maintained under natural sunlight, air  
253 temperature and humidity. Ten months later, healthy uniform plants were transplanted into 35 L  
254 pots with the same soil mix and grown for 30 days in a walk-in growth chamber (expanded  
255 temperature range Model BDW80, Conviron, Canada) before measurements were collected in July,  
256 2017. The maximum PAR in the walk-in growth chamber was set to 1200  $\mu\text{mol m}^{-2} \text{s}^{-1}$ . We planted  
257 two cotton species for this study. Cotton seeds were planted in 10 L pots using the standard potting  
258 mix on October 6, 2017 in a greenhouse. Supplemental lighting was turned on for 14h per day  
259 using HPS 1000 W growth lights that maintained light inside the greenhouse above  $\sim 400 \mu\text{mol m}^{-2}$   
260  $\text{s}^{-1}$ . Greenhouse air temperatures were set to 28 °C for the 14 h photoperiod and 25 °C at night.  
261 After 60 days, the plants were moved to the growth chamber for targeted measurements under

262 carefully controlled diurnal environmental conditions. After 14 days of acclimation, the topmost  
 263 fully expanded leaves on the main stem were selected for experiments. All species at ORNL were  
 264 irrigated and fertilized periodically with 20-10-20 NPK fertilizer (Southern AG, USA).

265 **Table 1.** Description of plant species, the corresponding Plant Functional Types (PFTs),  
 266 growth stage, and location.

Plant Types (PFTs)	Functional Species	Plant growth stage	Measured temperature (°C)	Location
Broadleaf tree-boreal (BDT Boreal)	<i>Betula alleghaniensis</i> (BA)	Mature plant	25	CBG
	<i>Betula papyrifera</i> (BP)	Mature plant	25	CBG
C <sub>3</sub> Grass	<i>Dichanthelium clandestinum</i> (DC)	Mature plant	25	CBG
Broadleaf shrub-temperate (BDS Temperate)	<i>Cornus racemosa</i> 'Cuyzam' (CRC)	Mature plant	25	CBG
	<i>Viburnum dentatum</i> 'Christom' (VD)	Mature plant	25	CBG
	<i>Cornus racemosa</i> 'Ottzam' (CRO)	Mature plant	25	CBG
Broadleaf tree-temperate (BDT Temperate)	<i>Juglans nigra</i> (JN)	Mature plant	25	CBG
	<i>Carya ovata</i> 'Wilcox' (CAO)	Mature plant	25	CBG
	<i>Liquidambar styraciflua</i> 'Moraine' (LSM)	Mature plant	25	CBG

	<i>Quercus shumardii</i> Buckl. (QUSH)	Seedlings	20, 25, 30, 35, 40, 45	ORNL
	<i>Quercus falcata</i> Michx. (QUFA)	Seedlings	20, 25, 30, 35, 40, 45	ORNL
	<i>Liriodendron tulipifera</i> L. (LITU)	Seedlings	20, 25, 30, 35, 40, 45	ORNL
<hr/>				
Needleleaf evergreen				
tree-Boreal	<i>Pinus strobus</i> L. (PIST)	Seedlings	25	ORNL
(NET Boreal)				
<hr/>				
C <sub>3</sub> Crops	<i>Gossypium hirsutum</i> L. (GH)	Flowering Stage	25	ORNL
	<i>Gossypium barbadense</i> L. (GB)	Flowering Stage	25	ORNL
<hr/>				

267

## 268 Measurement protocols of leaf gas exchanges and ChlF parameters

269 We measured both light and CO<sub>2</sub> response curves of gas exchanges and ChlF for each species at  
270 CBG and ORNL. For each curve, we selected three to five healthy and fully expanded leaves as  
271 replicates of each species. At CBG, curves were measured with GFS-3000 (Walz, Effeltrich,  
272 Germany) equipped with fluorescence measuring head (3010-S, Walz). At ORNL, these curves  
273 were measured with LI-6800 (LI-COR Inc., Lincoln, NE, USA) equipped with leaf multiphase  
274 flash fluorometer chamber (6800-01A, LI-COR Inc). For GFS-3000, RH was kept between 50%  
275 and 60%, the flow rate at 700 mL min<sup>-1</sup>, and the leaf temperature at 25 °C. Prior to actual  
276 measurements of light and CO<sub>2</sub> response curves, photosynthesis was first induced with a saturating  
277 light intensity. Once the steady state was reached (usually within 20 minutes), the auto-progress

278 of light and CO<sub>2</sub> response curve was adopted. We performed light response curve measurements  
279 following a sequence of PAR intensities: 2000, 1800, 1500, 1200, 1000, 800, 500, 300, 200, 150,  
280 100, 50, 0 μmol photon m<sup>-2</sup> s<sup>-1</sup> respectively, with CO<sub>2</sub> concentration in the leaf chamber provided  
281 by a CO<sub>2</sub> cylinder maintained constant at 400 μmol mol<sup>-1</sup>. Following the light response curve  
282 measurements, we collected CO<sub>2</sub> response curves on the same leaves following a sequence of CO<sub>2</sub>  
283 concentrations: 400, 300, 200, 150, 100, 50, 0, 380, 550, 800, 1000, 1200, 1500 μmol CO<sub>2</sub> mol<sup>-1</sup>  
284 under the saturated light intensity (2000 μmol m<sup>-2</sup> s<sup>-1</sup> for species at CBG; 1200 and 1500 μmol m<sup>-2</sup>  
285 s<sup>-1</sup> for species at ORNL). These light and CO<sub>2</sub> response curves were measured at 25°C, the  
286 reference temperature commonly used for standardizing photosynthetic parameters. Furthermore,  
287 for each individual leaf within a subset of plant species (LITU, QUSH, and QUFA) grown in the  
288 walk-in growth chamber at ORNL, we collected additional light and CO<sub>2</sub> response curves of gas  
289 exchanges and ChlF parameters under different leaf temperatures, 20, 25, 30, 35, 40, and 45 °C,  
290 respectively, with the same protocols described above.

291 After collecting the light and CO<sub>2</sub> response curves, which can be used to obtain gas  
292 exchange variables (*i.e.*, the intercellular CO<sub>2</sub> concentration -  $C_i$ ) and steady-state and maximum  
293 ChlF under light conditions ( $F_s$  and  $F_m'$ ), we subsequently measured the maximum and minimum  
294 ChlF under fully dark-adapted conditions ( $F_m$  and  $F_o$ ) for each leaf replicate under 25 °C. To  
295 achieve this, we first marked the measured area of each dark-adapted leaf to keep the same  
296 measuring position as during the response curve measurements. We wrapped the measured leaf  
297 with aluminum foil, dark-adapted it for at least half an hour, and then recorded  $F_o$  and  $F_m$ . The  
298 responses of  $F_m$  and  $F_o$  on temperatures (Pospisil *et al.*, 1998) were used to obtain the values of  
299  $F_m$  and  $F_o$  at other temperatures (20, 30, 35, 40, and 45 °C) in LITU, QUSH, and QUFA.

300 **Derivation of ChlF related variables**

301 The measured ChlF parameters were in turn used to calculate the following ChlF related variables,  
 302 including minimum ChlF under light ( $F_o'$ ),  $q_L$ , non-photochemical quenching (NPQ),  $SIF_{PSII}$  and  
 303 the actual electron transport rate ( $J_a$ ). Specifically:

304 
$$F_o' = \frac{F_o}{\Phi_{PSII_{max}} + \frac{F_o}{F_m'}} \quad (\text{Oxborough \& Baker, 1997}) \quad (\text{eqn 10})$$

305 where  $\Phi_{PSII_{max}}$  denotes the maximum photochemical yield in the dark-adapted leaves calculated as  
 306  $(F_m - F_o)/F_m$ .

307 
$$q_L = \frac{F_m' - F_s}{F_m' - F_o'} \times \frac{F_o'}{F_s} \quad (\text{Kramer } et al., 2004) \quad (\text{eqn 11})$$

308 11)

309 
$$NPQ = \frac{F_m - F_m'}{F_m'} \quad (\text{Genty } et al., 1989) \quad (\text{eqn 12})$$

310 12)

311 Then the leaf-level  $SIF_{PSII}$  was computed from the following theoretical equations (Porcar-  
 312 Castell *et al.*, 2014; Gu *et al.*, 2019):

313 
$$SIF_{PSII} = \Phi_{SIF} \times PAR \times \alpha \times \beta \quad (\text{eqn 13})$$

314 
$$\Phi_{SIF} = \frac{1 - \Phi_{PSII_{max}}}{(1 + k_{DF}) \times [(1 + NPQ) \times (1 - \Phi_{PSII_{max}}) + q_L \times \Phi_{PSII_{max}}]} \quad (\text{eqn 14})$$

315 14)

316 where  $\alpha$  is leaf absorptance and assumed to be 0.84 (Björkman & Demmig, 1987, Schreiber, 2004);  
 317  $\beta$  the fraction of light allocated to PSII, assumed to be 0.5 (von Caemmerer, 2000). It is assumed  
 318 here that  $k_{DF}$  is 10 according to the suggestion of Pfündel (1998) rather than 19 adopted by Gu *et*

319 *al.* (2019). The rationale is that the magnitude and range of  $\Phi_{\text{SIF}}$  calculated with a  $k_{\text{DF}}$  value of 10  
320 (eqn 14) could match the absolute fluorescence yield directly measured by Tesa *et al.* (2018).

321

322 Further,  $J_a$  was calculated with eqn 1 from  $SIF_{\text{PSII}}$  and  $q_L$  or directly from PAM parameters  
323 (Genty *et al.*, 1989; Schreiber, 2004; Gu *et al.*, 2019):

$$324 \quad J_a = \frac{F'_m - F_s}{F'_m} \times \text{PAR} \times \alpha \times \beta \quad (\text{eqn}$$

325 15)

326 The  $J_a$  formulations for eqn 1 and eqn 15 are theoretically identical although they use different  
327 parameters as inputs (Gu *et al.*, 2019).

### 328 **Estimation of $V_{\text{cmax}}$ and $J_{\text{max}}$**

329 We did not employ the theoretical formulations (eqn 5-6 and eqn 8-9) to directly calculate  $V_{\text{cmax}}$   
330 and  $J_{\text{max}}$  in this study, as the actual values of the input parameters (*e.g.*,  $\Gamma^*$ ,  $K_{\text{CO}}$ ,  $k_{\text{DF}}$ ,  $\theta$ , and  $\sigma$ ) are  
331 currently unknown although they have been considered as constants (note the validity of these  
332 equations were still validated in Note S2). Instead, to estimate  $V_{\text{cmax}}$  and  $J_{\text{max}}$ , we adopted the  
333 traditional approach, *i.e.*, fitting  $\text{CO}_2$  response curves based upon the FvCB model (Farquhar *et*  
334 *al.*, 1980; Sharkey, 1985) using the *photosynthesis* R package (Stinziano *et al.*, 2020). This  
335 approach adopts the fitting strategy of Gu *et al.* (2010), which iterates all possible  $C_i$  transitional  
336 points in order to automate the determination of the carboxylation limitation state, removal of  
337 inadmissible curves fits, and selection of the best fit by minimizing the cost function. Default  
338 parameters (*i.e.*,  $\Gamma^*$ ,  $K_c$ , and  $K_o$ ) and temperature response function were all from Bernacchi *et al.*  
339 (2001). Mesophyll conductance was assumed to be infinite for the present study (its limitation

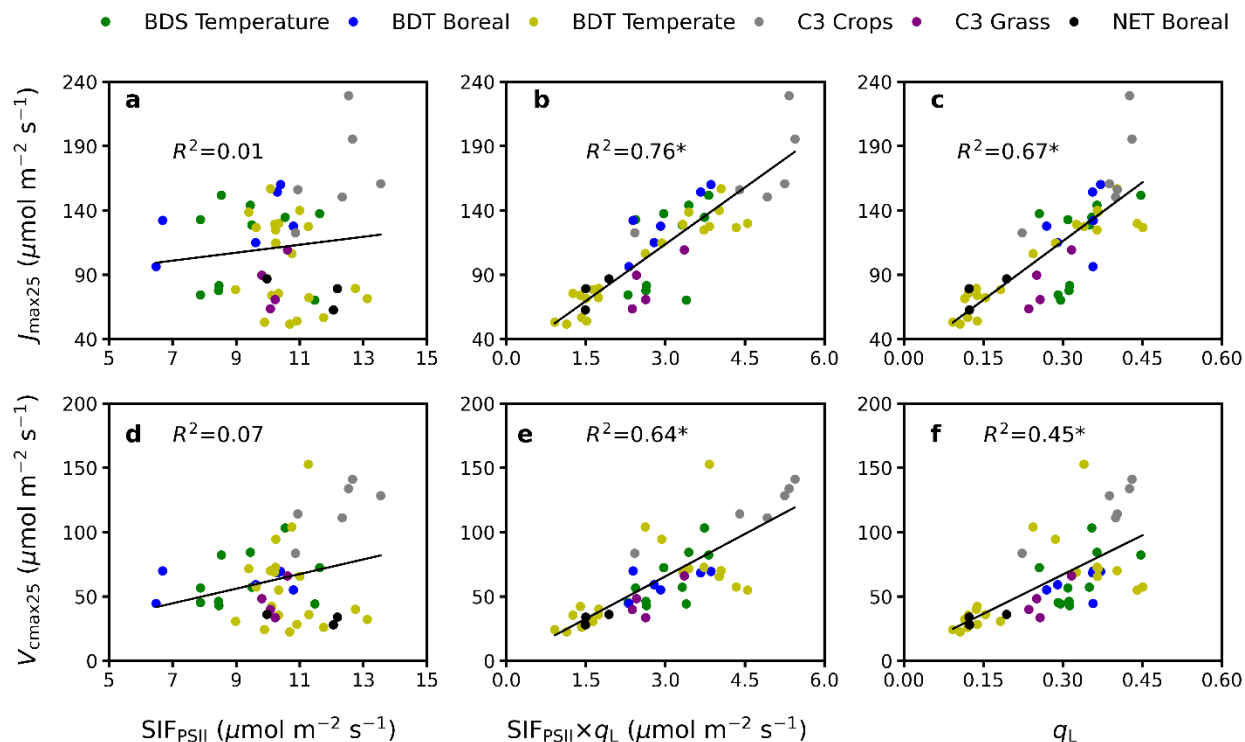
340 discussed in Notes S2). By default, this *photosynthesis* R package does not output the actual  
341 carboxylation limitation state, we thus conducted forward simulations of FvCB with the fitted  
342 parameter along with PAR and CO<sub>2</sub> concentration, and used the resulting minimal carboxylation  
343 rate as the output actual limiting state. We repeated this procedure for each leaf replicate under  
344 their measured temperatures. To better distinguish from  $V_{\text{cmax}25}$  and  $J_{\text{max}25}$ ,  $V_{\text{cmax}}$  and  $J_{\text{max}}$  at  
345 measuring leaf temperatures in the following content were denoted by  $V_{\text{cmax-T}}$  and  $J_{\text{max-T}}$ ,  
346 respectively.

## 347 Results

### 348 *Relationships of photosynthetic capacity parameters with $SIF_{PSII}$ , $q_L$ , and $SIF_{PSII} \times q_L$* 349 *(Hypotheses I and II)*

350 We first evaluated the relationships between photosynthetic capacity parameters ( $V_{cmax25}$  and  $J_{max25}$ )  
351 and  $SIF_{PSII}$  derived from ChlF measurements across 15 different plant species (grouped into six  
352 PFTs) under the light intensity of  $1200 \mu\text{mol m}^{-2} \text{s}^{-1}$ , ambient  $\text{CO}_2$  concentration, and  $25^\circ\text{C}$ . We  
353 did not observe any detectable relationships between  $SIF_{PSII}$  and  $J_{max25}$  ( $R^2=0.01$ , Fig. **1a**) or  $V_{cmax25}$   
354 ( $R^2=0.07$ , Fig. **1d**). This suggests that  $SIF_{PSII}$  itself alone is unable to capture the variation of  $V_{cmax25}$   
355 and  $J_{max25}$  across plant species, even under strictly controlled environmental conditions. In contrast,  
356 once  $q_L$  variation is accounted for, we found striking relationships between  $SIF_{PSII} \times q_L$  and both  
357 photosynthetic capacity parameters, *i.e.*,  $R^2 = 0.76$  ( $p < 0.05$ ) for  $J_{max25}$  and  $R^2 = 0.64$  ( $p < 0.05$ ) for  
358  $V_{cmax25}$  respectively (Fig. **1b,e**).  $q_L$  itself is also significantly related to  $J_{max25}$  ( $R^2=0.67$ ,  $p < 0.05$ ,  
359 Fig. **1c**) and  $V_{cmax25}$  ( $R^2=0.45$ ,  $p < 0.05$ , Fig. **1f**) across plant species. However, compared to  
360  $SIF_{PSII} \times q_L$ , the explanatory power of  $q_L$  for  $J_{max25}$  and  $V_{cmax}$  is reduced by 12% and 30%,  
361 respectively. These patterns suggest that  $SIF_{PSII} \times q_L$  is a much more effective predictor to infer  
362 photosynthetic capacity parameters than  $SIF_{PSII}$  or  $q_L$  itself alone. This is because  $SIF_{PSII} \times q_L$  not  
363 only contains the information of fluorescence emissions, but also, implicitly, that of NPQ  
364 dynamics which regulates the relationships of  $SIF_{PSII}$  with photosynthetic capacity, according to  
365 the principle of energy balance (*i.e.*, eqn 20 in Gu *et al.*, 2019, more details in Discussions). Our  
366 results directly drawn from measurements confirm our Hypothesis I and II formulated from  
367 theoretical reasoning. Still the  $SIF_{PSII} \times q_L - V_{cmax}/J_{max}$  relationships can to some degree vary across  
368 PFTs (Fig. 1), likely a consequence of other parameters that were assumed to be constant but can

369 differ among plant species (e.g.,  $\Gamma^*$  and  $K_{co}$  in eqn 5, detailed discussions in Notes S2) and the  
 370 specific growth conditions in natural environments (e.g., varying climates, soil conditions,  
 371 topography, among others, detailed discussion below).

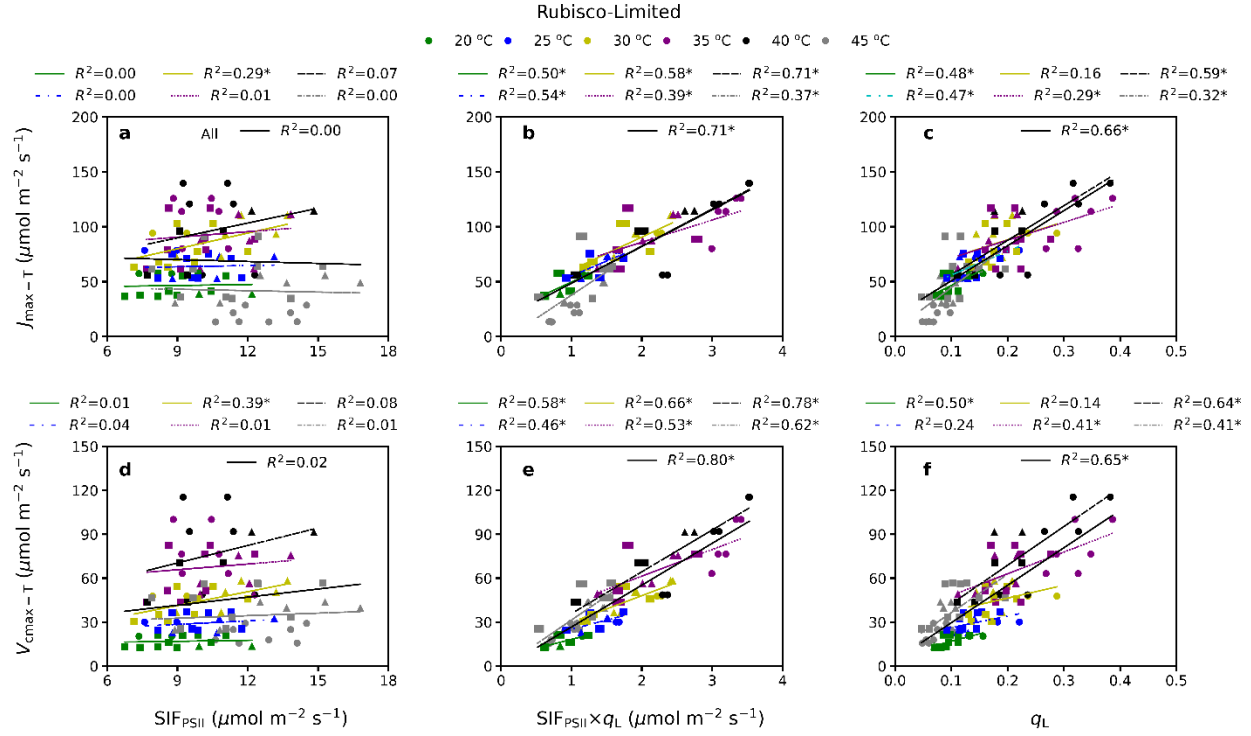


372 **Fig. 1.** The relationships of  $SIF_{PSII}$  with  $J_{max25}$  (a) and  $V_{cmax25}$  (d), the relationships of  
 373  $SIF_{PSII} \times q_L$  with  $J_{max25}$  (b) and  $V_{cmax25}$  (e), and the relationships of  $q_L$  with  $J_{max25}$  (c) and  $V_{cmax25}$   
 374 (f) respectively, across 15 plant species grouped into six plant function types (PFTs, Table 1).  
 375 Here,  $SIF_{PSII}$  was calculated with the ChlF parameters (eqn 13) at PAR of  $1200 \mu\text{mol m}^{-2} \text{s}^{-1}$ ,  
 376 ambient  $\text{CO}_2$  concentration ( $400 \mu\text{mol mol}^{-1}$ ), and  $25^\circ\text{C}$ .  $J_{max25}$  and  $V_{cmax25}$  were fitted with the  
 377 FvCB model at  $25^\circ\text{C}$ . Each scatter represents one leaf replicate, color coded by PFTs. The  
 378 black lines are linear ordinary least-square regression with all leaves pooling together. \*  
 379 denotes a statistically significant at the significance level of 0.05.

381

382 **Impact of temperature variations on the relationships of photosynthetic capacity parameters**  
383 **with  $SIF_{PSII}$ ,  $q_L$ , and  $SIF_{PSII} \times q_L$  (Hypothesis III)**

384 For a subset of plant species, light and CO<sub>2</sub> response curves were collected under varying  
385 temperatures ranging from 20 °C to 45 °C (Table 1). For these species, we found that under the  
386 Rubisco-limited state,  $J_{\max-T}$  ( $V_{\max-T}$ ) can be either positively or negatively correlated with  $SIF_{PSII}$   
387 (under the same temperature) as temperature varies, and none of their relationships are statistically  
388 significant except for the correlation at 30 °C (Fig. **2a,d**). In contrast, there are strong correlations  
389 of  $SIF_{PSII} \times q_L$  with  $J_{\max-T}$  ( $R^2=0.71$ ) and with  $V_{\max-T}$  ( $R^2=0.80$ ) when all plant species are pooled  
390 together (Fig. **2b,e**). Also,  $q_L$  is significantly related to  $J_{\max-T}$  and  $V_{\max-T}$ , with 66% and 65% of  
391 the variability of  $J_{\max-T}$  (Fig. **2c**) and  $V_{\max-T}$  (Fig. **2f**) being explained by  $q_L$ . The relationships  
392 between  $SIF_{PSII} \times q_L$  and  $J_{\max-T}$  ( $V_{\max-T}$ ) are stronger than that between  $q_L$  and  $J_{\max-T}$  ( $V_{\max-T}$ ) at a  
393 single temperature or across all the temperatures. This indicates that  $SIF_{PSII}$  alone, to a certain  
394 extent, can constraint (not accurately estimate though) the variability of photosynthetic capacity  
395 parameters across plant species.  $SIF_{PSII} \times q_L$  can infer photosynthetic capacity parameters more  
396 accurately than  $SIF_{PSII}$  or  $q_L$  itself alone across temperatures. Interestingly, the regression slopes  
397 of  $SIF_{PSII} \times q_L$  (Fig. **2b,e**) against  $J_{\max-T}$  ( $V_{\max-T}$ ) are relatively stable across a broad range of  
398 temperature variation under Rubisco limitation.

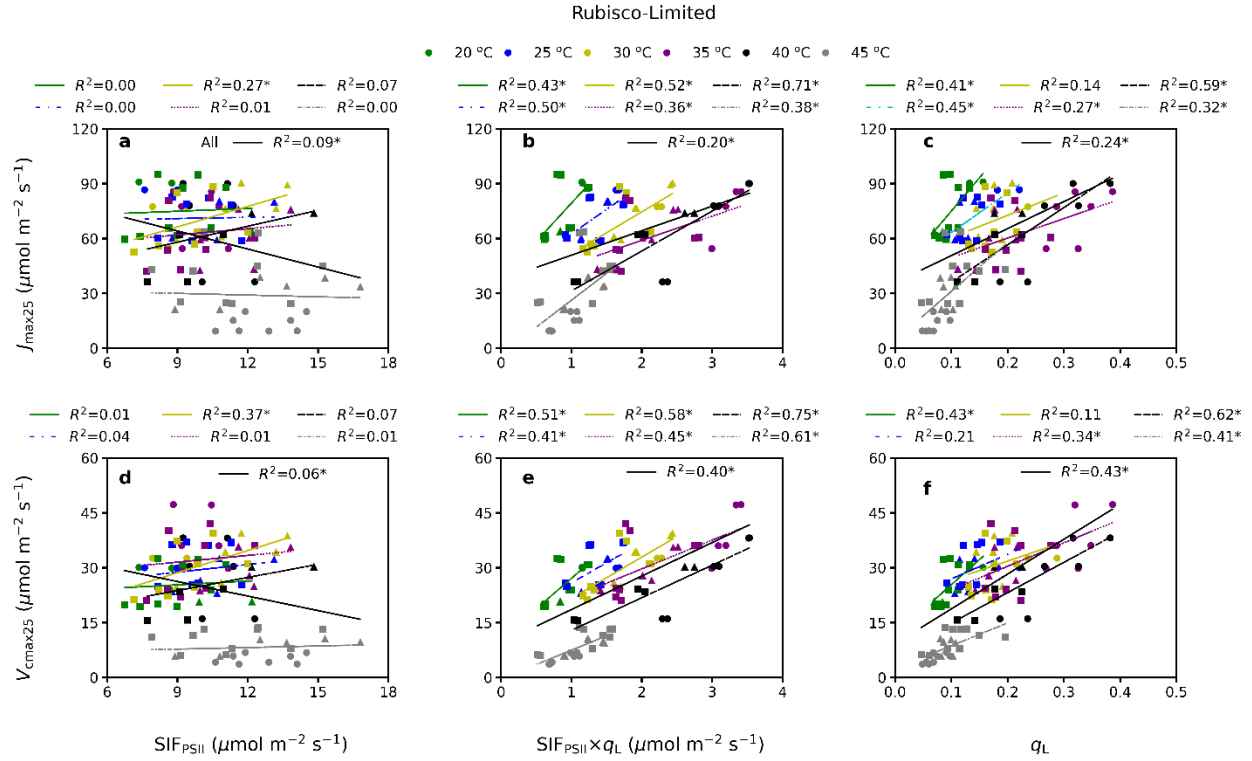


399

400 **Fig. 2.** Impact of temperature variations on the relationship of  $J_{\max-T}$  (and  $V_{\text{cmax-T}}$ ) with  $SIF_{\text{PSII}}$   
 401 (a, d),  $SIF_{\text{PSII}} \times q_L$  (b, e), and  $q_L$  (c, f). Similar to Fig.1, but the relationships were analyzed under  
 402 Rubisco-limited state for a subset of plant species that were measured under different  
 403 temperatures, *i.e.* 20 °C (n = 14), 25 °C (n = 16), 30 °C (n = 16), 35 °C (n = 20), 40 °C (n = 12),  
 404 45 °C (n = 24).  $SIF_{\text{PSII}}$  and  $SIF_{\text{PSII}} \times q_L$  were calculated with eqn 13 under the PAR of 1200 and  
 405 1000  $\mu\text{mol m}^{-2} \text{s}^{-1}$ . The data size (n) depends on how many data samples were Rubisco-limited  
 406 under each temperature.  $J_{\max-T}$  and  $V_{\text{cmax-T}}$  were fitted with the FvCB model at these individual  
 407 temperatures. Each scatter represents one single leaf, separated by plant species (circle: LITU,  
 408 triangle: QUSH, square: QUFA), and grouped by temperature.

409 When normalizing  $J_{\max-T}$  (and  $V_{\text{cmax-T}}$ ) to the reference temperature 25 °C, their strong  
 410 correlation with  $SIF_{\text{PSII}} \times q_L$  remains relatively stable but their regression slopes diverge  
 411 considerably (Fig. 3b,e). This pattern suggests that, under the Rubisco limitation, temperature

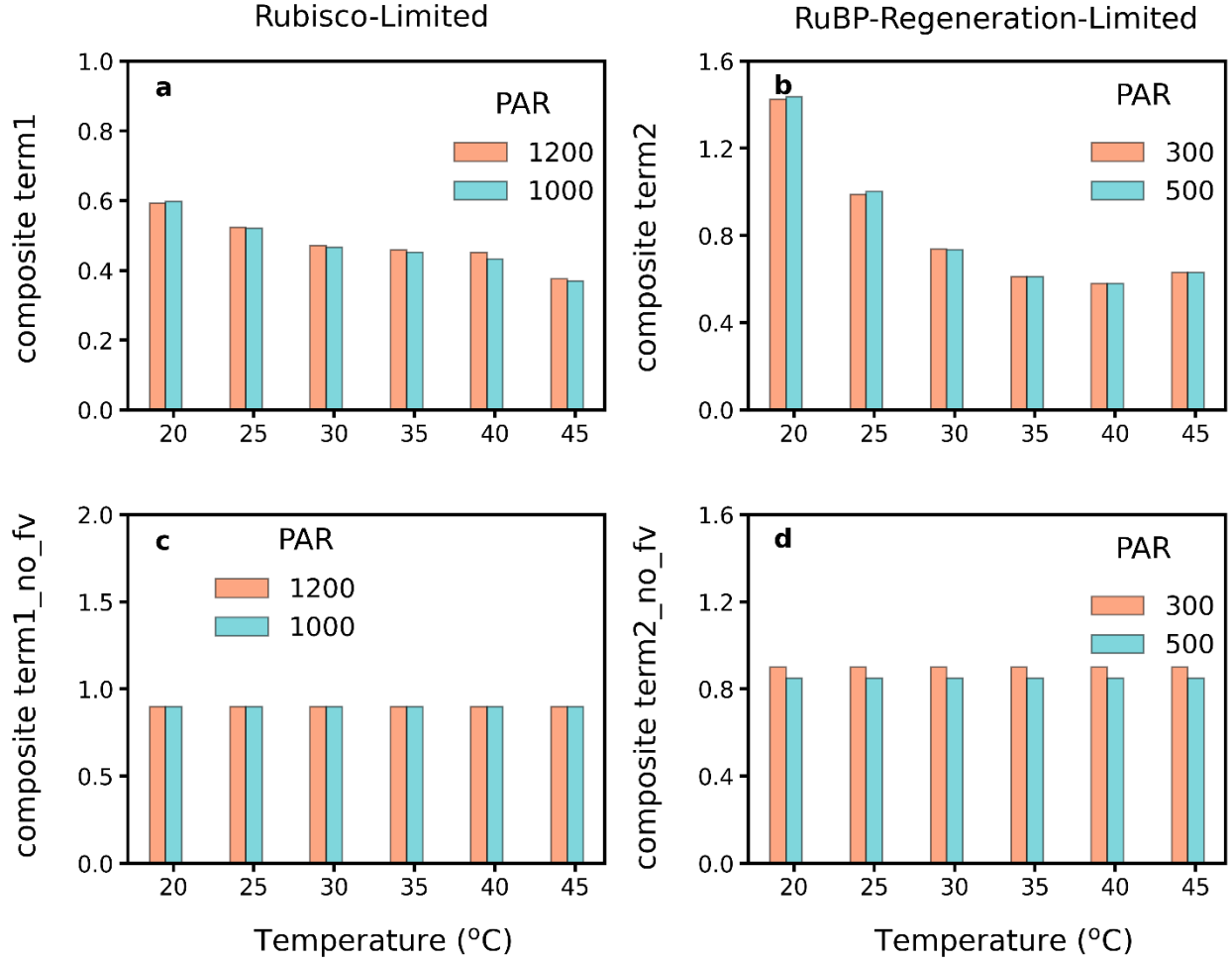
412 variations can further complicate the relationships of  $V_{\text{cmax}25}$  and  $J_{\text{max}25}$  with  $SIF_{\text{PSII}} \times q_L$ , confirming  
413 our Hypothesis III. Such divergence of regression slopes is likely a consequence of the regulation  
414 of  $f_V(T)$  and  $f_J(T)$ . This is supported by Fig. 4, which shows the composite terms  $(\frac{C_i + K_{co}}{4C_i + 8\Gamma^*})$  and  
415  $\theta \cdot \frac{q_L \cdot SIF_{\text{PSII}} \cdot (1 + k_{DF})}{\sigma \cdot PAR} - \frac{1 - \Phi_{\text{PSII}max}}{\Phi_{\text{PSII}max}}$  in eqn 8 and 9 respectively are relatively stable across different  
416 temperatures (Fig. 4c,d), compared to if when  $f_V(T)$  and  $f_J(T)$  are included (Fig. 4a,b). This  
417 analysis mimics the actual applications of remote sensing  $SIF$  (measured under dynamic  
418 temperatures) for inferring  $V_{\text{cmax}25}$  and  $J_{\text{max}25}$ . In addition, a weaker relationship of  $J_{\text{max}25}$  (and  
419  $V_{\text{cmax}25}$ ) with  $q_L$  than with  $SIF_{\text{PSII}} \times q_L$  was observed under each temperature (Fig. 3b, e versus Fig.  
420 3c, f). However, when all the data at different temperatures were pooled together, the explanatory  
421 power of  $SIF_{\text{PSII}} \times q_L$  for  $J_{\text{max}25}$  and  $V_{\text{cmax}25}$  is similar to or even lower than that of  $q_L$  alone. This  
422 indicates that  $SIF_{\text{PSII}}$  cannot capture the variability of  $J_{\text{max}25}$  and  $V_{\text{cmax}25}$  caused by temperatures  
423 (also confirm by Fig. 5d below). Note the dependence of  $k_D$  on the temperature (van der Tol *et al.*,  
424 2014) may affect the response of  $SIF_{\text{PSII}}$  on temperatures, but  $k_D$  and  $k_F$  are fundamental physical  
425 properties of the chlorophyll molecule and there is current no physical mechanism to explain the  
426 dependence of  $k_D$  (an antenna process) on temperature.



427

428 **Fig. 3.** Similar to Fig.2 except  $V_{\text{cmax-T}}$  and  $J_{\text{max-T}}$  were normalized to 25 °C, *i.e.*, for  $V_{\text{cmax25}}$  and

429  $J_{\text{max25}}$ .



430

431 **Fig. 4.** The variations of the composite term of eqn 8 ( $\frac{1}{f_V(T)} \times \frac{C_i + Kco}{4C_i + 8\Gamma^*}$ , a;  $\frac{C_i + Kco}{4C_i + 8\Gamma^*}$ , c) and of eqn

432  $9 \left( \frac{1}{f_V(T)} \times \frac{\theta \cdot q_L \cdot SIF_{PSII} \cdot (1 + k_{DF})}{\sigma \cdot PAR} - \frac{1 - \Phi_{PSII_{max}}}{\Phi_{PSII_{max}}} \right)$ , b;  $\frac{\theta \cdot q_L \cdot SIF_{PSII} \cdot (1 + k_{DF})}{\sigma \cdot PAR} - \frac{1 - \Phi_{PSII_{max}}}{\Phi_{PSII_{max}}}$ , d) with (a,b) and

433 without (b,d) the consideration of temperature function under different temperatures. Different

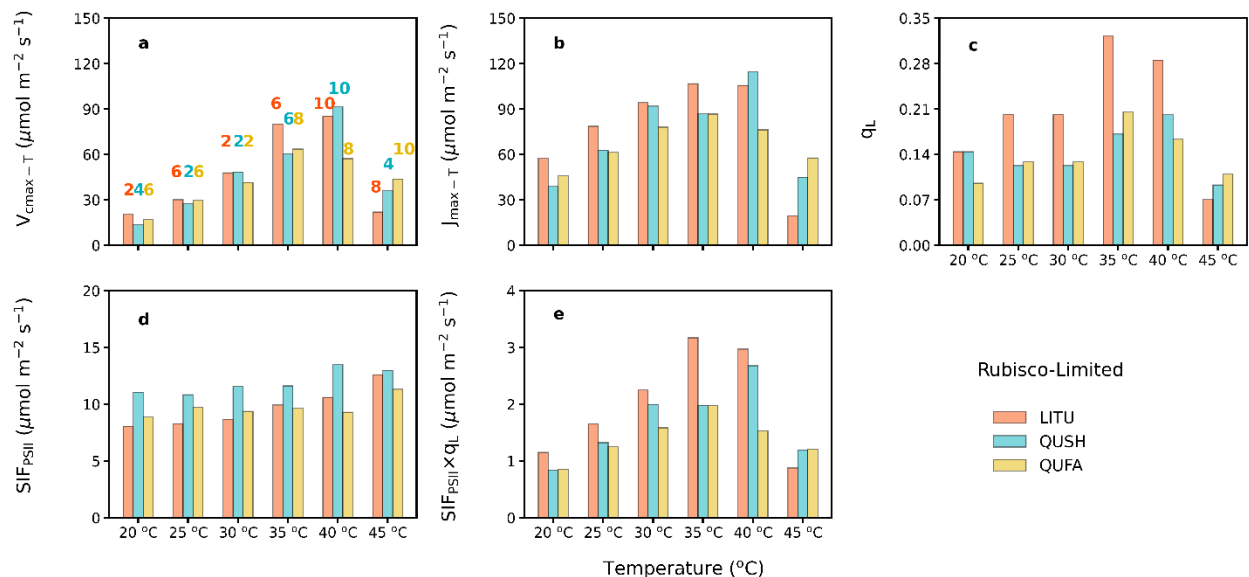
434 colors represent different PAR. Each bar represents the mean of all the replicate individuals in

435 three species (LITU, QUSH, and QUFA).

436 To understand why the  $SIF_{PSII} \times q_L \sim V_{c_{max-T}} (J_{max-T})$  relationships can hold relatively stable

437 across temperatures under the Rubisco limitation, we compared the temperature dependence of

438  $SIF_{PSII}$  with those of  $q_L$ , and  $V_{cmax-T}$  ( $J_{max-T}$ ) (Fig. 5). We found that temperatures have stronger  
 439 impact on  $q_L$  and  $V_{cmax-T}$  ( $J_{max-T}$ ) than on  $SIF_{PSII}$ . For example, for all species,  $q_L$  and  $V_{cmax-T}$  ( $J_{max-T}$ )  
 440 increase almost in parallel as a function of temperature from 20°C to 35°C and then both declined  
 441 at higher temperatures (Fig. 5a,b,c). Such consistency in the variations of  $q_L$  and  $V_{cmax-T}$  ( $J_{max-T}$ )  
 442 with temperatures implies that  $q_L$  can reflect the activation of the carboxylation enzyme. In contrast,  
 443  $SIF_{PSII}$  does not exhibit much variation with temperature (Fig. 5d), likely a consequence of the  
 444 dominant role of light on  $SIF_{PSII}$ . Collectively, the product of  $SIF_{PSII}$  and  $q_L$  can effectively  
 445 characterize the temperature impacts on  $V_{cmax-T}$  ( $J_{max-T}$ ) (Fig. 5e).



446  
 447 **Fig. 5.** The variations of  $V_{cmax-T}$  (a),  $J_{max-T}$  (b),  $q_L$  (c),  $SIF_{PSII}$  (d), and  $SIF_{PSII} \times q_L$  (e) under different  
 448 temperatures for three species (LITU, QUSH, QUFA). Each bar represents the mean of leaf  
 449 replicates within the same temperature under the Rubisco limited state, the number of replicates is  
 450 shown above each bar.

451 **Carboxylation limitation states must be considered for using  $SIF_{PSII}$  to infer photosynthetic**  
 452 **capacity parameters (*Hypothesis IV*)**

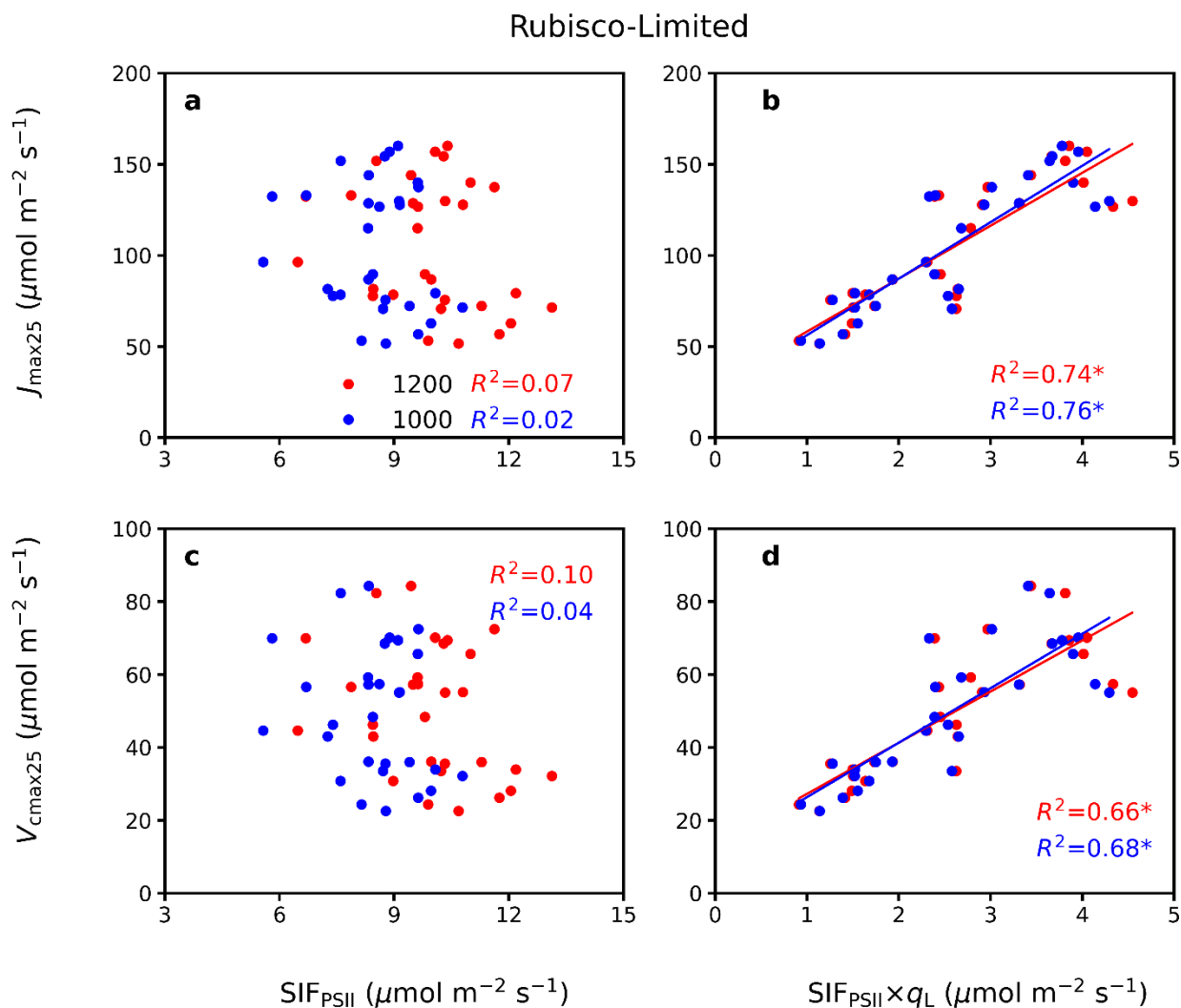
453 As  $SIF_{PSII}$  (and also  $q_L$ ) varies instantaneously with PAR while photosynthetic capacity parameters  
 454 have no dependence on PAR, we further examined whether and how carboxylation limitation state  
 455 (which depends on PAR) alters the relationship between  $SIF_{PSII}$  (and  $SIF_{PSII} \times q_L$ ) and  $J_{\max 25}$  (and  
 456  $V_{\max 25}$ ). We found that  $SIF_{PSII} \times q_L$  is more tightly related to  $J_{\max 25}$  (and  $V_{\max 25}$ ) linearly under  
 457 Rubisco-limited state (when PAR = 1200 and 1000  $\mu\text{mol m}^{-2} \text{s}^{-1}$ ) than under RuBP regeneration-  
 458 limited state (when PAR = 500 and 300  $\mu\text{mol m}^{-2} \text{s}^{-1}$ ) (comparing Fig. **6b,d** and Fig. **7b,d**). Again,  
 459  $SIF_{PSII}$  alone does not appear to have any significant relationship with  $J_{\max 25}$  or  $V_{\max 25}$ , regardless  
 460 of the carboxylation limiting states (Fig. **6a,c** and Fig. **7a,c**). These findings confirm our  
 461 Hypothesis IV.

462 Moreover, the regression slopes of  $J_{\max 25}$  (or  $V_{\max 25}$ ) against  $SIF_{PSII} \times q_L$  are similar between  
 463 1200 and 1000  $\mu\text{mol m}^{-2} \text{s}^{-1}$  ( $p = 0.683$  for  $J_{\max 25}$ ,  $p = 0.743$  for  $V_{\max 25}$ , based on two tail  $t$ -test),  
 464 both under the Rubisco-limited state (Fig. **6b,d**). To verify this result with theoretical formula, we  
 465 checked the composite term of  $\frac{1}{f_V(T)} \times \frac{C_i + K_{co}}{(4C_i + 8\Gamma^*)}$  (eqn 8) under different PAR levels, and found that  
 466 PAR indeed has minimal impact on the magnitude of this composite term across all temperatures  
 467 (Fig. **4a**). However, this term is highly sensitive to temperature variations, explaining the divergent  
 468  $J_{\max 25}$  (or  $V_{\max 25}$ )  $\sim SIF_{PSII} \times q_L$  regression slopes across temperatures (Fig. **3b,d**). Under the RuBP  
 469 regeneration limitation, there is also no significant difference in the regression slopes of  $J_{\max 25}$  (or  
 470  $V_{\max 25}$ ) against  $SIF_{PSII} \times q_L$  between 500 and 300  $\mu\text{mol m}^{-2} \text{s}^{-1}$  ( $p = 0.725$  for  $J_{\max 25}$ ,  $p = 0.609$  for  
 471  $V_{\max 25}$ ) (Fig. **7b,d**). This can be supported by Fig. **4b**, in which PAR has negligible impact on the

472 composite term of  $\frac{1}{f_V(T)} \times \frac{\theta \cdot \frac{q_L \cdot SIF_{PSII} \cdot (1 + k_{DF})}{\sigma \cdot PAR} - \frac{1 - \Phi_{PSII\max}}{\Phi_{PSII\max}}}{\frac{q_L \cdot SIF_{PSII} \cdot (1 + k_{DF})}{\sigma \cdot PAR} - \frac{1 - \Phi_{PSII\max}}{\Phi_{PSII\max}}}$  (eqn 9) across all temperatures. Similar

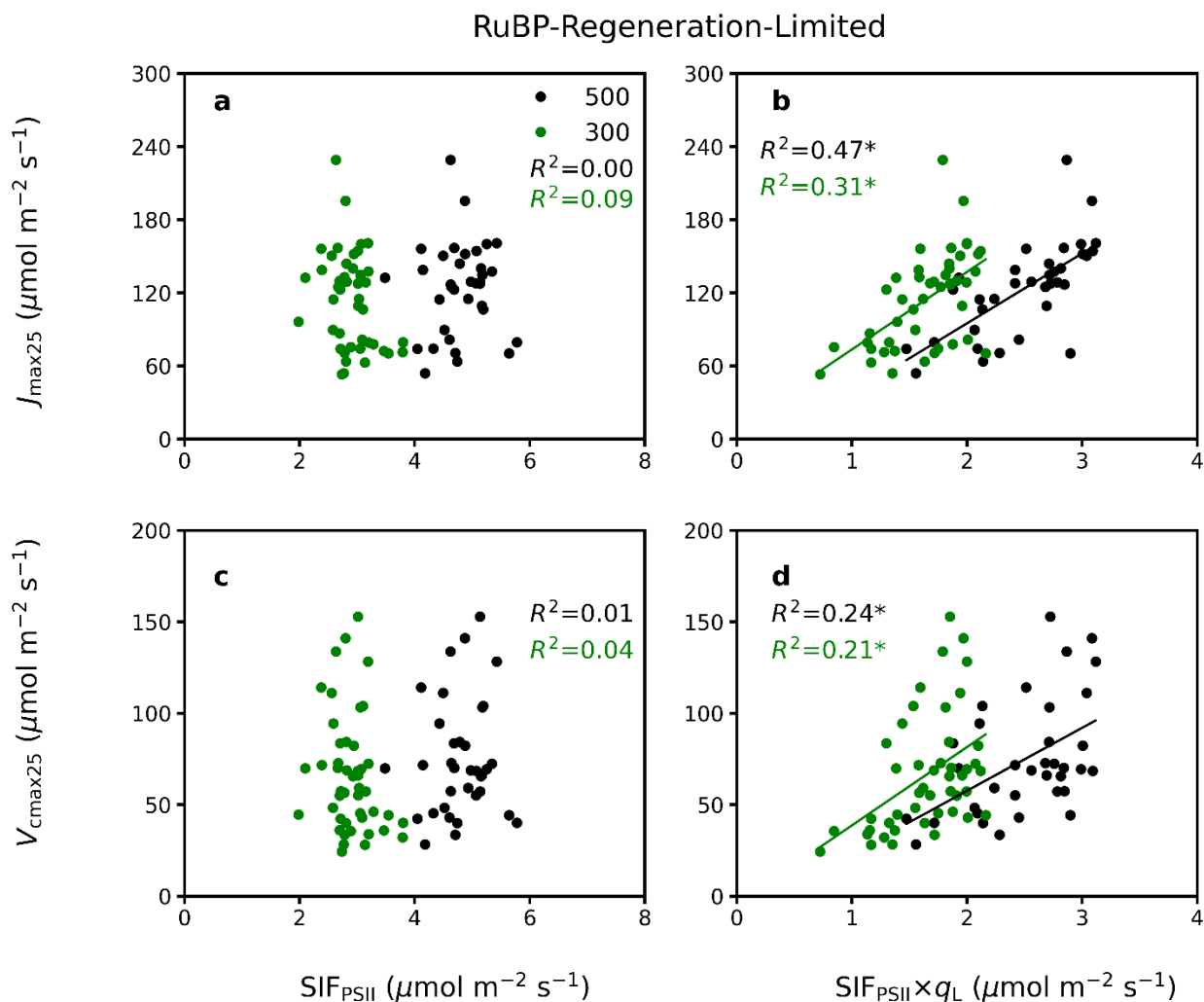
473 to the composite term in eqn 8, the composite term in eqn 9 is considerably affected by  
474 temperatures.

475 In contrast, the regression slopes of  $V_{\text{cmax}25}$  (or  $J_{\text{max}25}$ ) against  $SIF_{\text{PSII}} \times q_L$  under the Rubisco  
476 limitation differ significantly from that under RuBP regeneration limitation when a single PAR for  
477 each limitation is considered (*i.e.*, 1200 vs 500, 1200 vs 300, 1000 vs 500, 1000 vs 300). These  
478 results suggest that prior information of photosynthetic limitation stage should be considered when  
479 observational  $SIF_{\text{PSII}}$  (or SIF) is employed to infer photosynthetic capacity parameters.



480

481 **Fig. 6.** Similar to Fig.1 but the relationships were analyzed under the Rubisco limitation only.  
 482  $SIF_{PSII}$  and  $SIF_{PSII} \times q_L$  were calculated with ChlF parameters that measured under the PAR of 1200  
 483 (red) and 1000 (blue)  $\mu\text{mol m}^{-2} \text{s}^{-1}$ . The linear ordinary least-square regressions were made for  
 484 each light intensity separately.



485  
 486 **Fig. 7.** Similar to Fig.1 but the relationships were analyzed under the RuBP regeneration limitation  
 487 only.  $SIF_{PSII}$  and  $SIF_{PSII} \times q_L$  were calculated with ChlF parameters measured under the PAR of 500  
 488 (black) and 300 (green)  $\mu\text{mol m}^{-2} \text{s}^{-1}$ . The linear ordinary least-square regressions were made for  
 489 each light intensity separately.

## 490 **Discussion**

### 491 **The product of $SIF_{PSII}$ and $q_L$ has greater capability for inferring photosynthetic capacity** 492 **than $SIF_{PSII}$ alone**

493 We observed prominent positive correlation of  $SIF_{PSII} \times q_L$  with both  $J_{\max 25}$  and  $V_{\max 25}$  across  
494 different species under various temperatures and PAR levels, demonstrating that  $SIF_{PSII} \times q_L$   
495 contains more information on physiological variations related to photosynthetic capacity than  
496  $SIF_{PSII}$  alone. This finding can be interpreted mechanistically with eqn 8 and eqn 9, derived by  
497 combining MLR-SIF (Gu *et al.*, 2019) and FvCB model (Farquhar *et al.*, 1980) under the  
498 assumption of light and carbon reaction balance.  $q_L$  reflects the redox state of the electron acceptors  
499 in PSII which is highly sensitive to electron transport (Kramer *et al.*, 2004; Baker, 2008). When  
500 there is an imbalance between the production of ATP/NADPH at the end of the light reactions and  
501 their consumption in the dark reactions which is affected by CO<sub>2</sub> diffusion and photosynthetic  
502 capacity, redox reaction rates along the electron transport chain are adjusted instantly (Johnson &  
503 Berry, 2021), affecting  $q_L$ . Additionally, thylakoid lumen can either acidify or alkalify, depending  
504 on the direction of imbalance. Changes in lumen acidity control the energy-dependent component  
505 of NPQ and the redox state of the plastoquinone pool (PQ/PQH<sub>2</sub>) (a rate-limiting step of electron  
506 transport), which is reflected by changes in  $q_L$  (Foyer *et al.*, 2012). Thus, the variation of  $q_L$  is a  
507 result of interactions between the light and carbon reactions, both of which respond to  
508 environmental variations (Rochaix, 2011; Roach & Krieger-Liszkay, 2014).

509 Note that since this study focuses on the functional relationships between  $SIF_{PSII}$  ( $q_L$ , and  
510  $SIF_{PSII} \times q_L$ ) and photosynthetic capacity parameters instead of their respective absolute values,  
511 potential measurement differences induced by instruments (*i.e.*, Li-6800 and GFS-3000) should

512 not affect our data analysis and conclusions. In addition, this study used modelled  $SIF_{PSII}$  (eqn 13),  
513 not the directly measured ChlF emission rate to infer photosynthetic capacity parameters. Our  
514 rationale is that, in theory,  $J_a$  required by MLR-SIF to estimate photosynthesis (and photosynthetic  
515 capacity parameters) should be calculated from the ChlF signal from PSII only (denoted as  $SIF_{PSII}$ )  
516 rather than that contains contributions from both PSII and PSI, which is usually the case for directly  
517 observed ChlF emission rate or remotely sensed SIF. Nevertheless, the modeled  $SIF_{PSII}$  was  
518 thoroughly evaluated with independent ChlF emission spectra elsewhere (Han *et al.*, 2021, under  
519 review). Also, we acknowledge that the assumed constants  $\alpha$ ,  $\beta$ , and  $k_{DF}$  in eqn 13 can potentially  
520 affect the calculation of  $SIF_{PSII}$ , but not the general patterns between photosynthetic capacities and  
521  $SIF_{PSII}$  (or  $SIF_{PSII} \times q_L$ ). For facilitating the broad applications of the approach calculating  $SIF_{PSII}$ ,  
522 the values of  $\alpha$ ,  $\beta$ , and  $k_{DF}$  need to be precisely determined in the future.

### 523 **Factors impacting the relationship between photosynthetic capacity parameters and** 524 **$SIF_{PSII} \times q_L$**

525 The precise relationships of  $SIF_{PSII} \times q_L$  with  $V_{cmax25}$  under the Rubisco limitation also depend on  
526  $C_i$  according to eqn 8. For broad applications,  $C_i$  is often assumed to be a constant ratio of ambient  
527  $CO_2$  concentration  $C_a$  (e.g.,  $C_i/C_a \sim 0.7$  in  $C_3$  species), but it changes with stomatal conductance  
528 which is affected directly by VPD and temperatures (Morison & Gifford, 1982). Indeed, the redox  
529 state of  $Q_A$ , measured by  $q_L$ , is a strong predictor of stomatal conductance (Busch, 2014; Glowacka  
530 *et al.*, 2018; Kromdijk *et al.*, 2019) and can partly explain the dynamic of stomatal conductance.  
531 Thus, modeling stomatal conductance with  $q_L$  in the future may eliminate the effects of  $CO_2$  on  
532  $SIF_{PSII} \times q_L \sim V_{cmax25}$  relationship. Additionally, to make the method of inferring  $V_{cmax25}$  ( $J_{max25}$ )  
533 with  $SIF_{PSII} \times q_L$  applicable beyond the leaf scale,  $q_L$  needs to be modelled as a function of

534 environments (*e.g.*, temperature, PAR, CO<sub>2</sub> levels, and nutrient stress) in future studies, given that  
 535 it cannot be directly measured at large scales. Under RuBP regeneration limitation,  $J_{\max25}$  and  
 536  $SIF_{\text{PSII}} \times q_L$  might not be linearly correlated, because the variables  $SIF_{\text{PSII}}$  and  $q_L$  are still involved  
 537 in the slope ( $\frac{1}{f_V(T)} \times \frac{\theta \cdot \frac{q_L \cdot SIF_{\text{PSII}} \cdot (1 + k_{\text{DF}})}{\sigma \cdot \text{PAR}} - \frac{1 - \Phi_{\text{PSIImax}}}{\Phi_{\text{PSIImax}}}}{\frac{q_L \cdot SIF_{\text{PSII}} \cdot (1 + k_{\text{DF}})}{\sigma \cdot \text{PAR}} - \frac{1 - \Phi_{\text{PSIImax}}}{\Phi_{\text{PSIImax}}}}$  in eqn 9). This further suggests the necessity  
 538 of modelling  $q_L$  in the future to explore the environmental factors influencing the relationships  
 539 between photosynthetic capacity parameters and  $SIF_{\text{PSII}} \times q_L$ .

540 Besides  $q_L$ , eqn 8 and 9 contains other parameters (*e.g.*,  $k_{\text{DF}}$ ,  $K_{\text{co}}$ ,  $I^*$ , and  $\Phi_{\text{PSIImax}}$ ). These  
 541 additional parameters are often assumed to be constant in literatures but in reality can vary across  
 542 plant species and growth environmental conditions (*e.g.*, temperature, water and nutrient stress,  
 543 and PAR). For example, the actual  $k_{\text{DF}}$  value is currently unknown. A value of 10 was implied in  
 544 Pfündel (1998) while Gu *et al.* (2019) set  $k_{\text{DF}}$  to 19. The use of these two  $k_{\text{DF}}$  values would directly  
 545 cause  $V_{\text{cmax25}}$  to vary by a factor of two according to eqn 8. Moreover, van der Tol *et al.* (2014)  
 546 speculated that  $k_{\text{D}}$  (an antenna process) depends on the temperature (even though there is currently  
 547 no physical mechanism to explain the dependence of  $k_{\text{D}}$  on temperatures), which can affect the  
 548 magnitude of calculated  $SIF_{\text{PSII}}$  and its response on temperatures. However, the variation of  $k_{\text{D}}$   
 549 caused by temperature does not impact the general relationship between  $SIF_{\text{PSII}}$  and  $V_{\text{cmax25}}$  (or  
 550  $J_{\max25}$ ) as  $k_{\text{DF}}$  remains unchanged under the same temperature and only  $SIF_{\text{PSII}}$  stratified to a certain  
 551 abiotic conditions (*e.g.*, same temperature) can be used to infer  $V_{\text{cmax25}}$  (demonstrated in Fig. 3).  
 552 Thus, our conclusion that the product of  $SIF_{\text{PSII}}$  and  $q_L$  has greater capability for inferring  
 553 photosynthetic capacity than  $SIF_{\text{PSII}}$  alone still holds true even if temperature has an impact on  $k_{\text{D}}$ .  
 554 In addition,  $K_{\text{co}}$  and  $I^*$  are related to the specificity factor of Rubisco, which depend on temperature  
 555 and the partial pressure of oxygen, and also varies among PFTs (refer to Notes S2). Furthermore,

556  $\Phi_{\text{PSII}_{\text{max}}}$  is relatively conservative ( $\sim 0.82$ ) across plant species but can decrease under stressed  
557 environmental conditions. Given these potential effects of varying environmental conditions, plant  
558 species, and growth status (*e.g.*, plant/leaf age, stress) on the parameters involved in our theoretical  
559 equations, and consequently the strength of the relationships between  $SIF_{\text{PSII}}$ ,  $SIF_{\text{PSII}} \times q_L$ , and  
560 photosynthetic capacity parameters, more measurements are required in the future to quantitatively  
561 examine their relationships across broad biotic and abiotic conditions.

562 **The discrepancies of the relationships between photosynthetic capacity parameters and SIF**  
563 **(or  $SIF_{\text{PSII}}$ ) among existing studies**

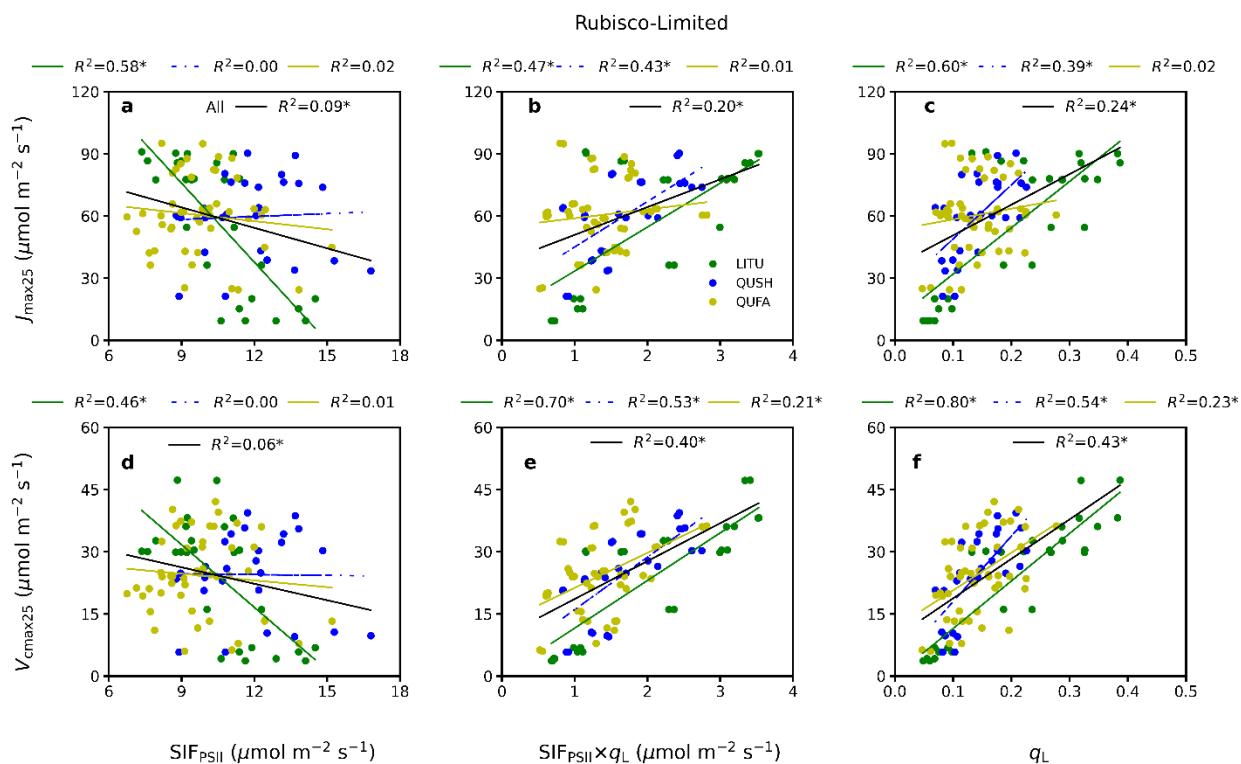
564 Our theoretical and measurement results consistently showed that no general, predictive  
565 relationships exist between photosynthetic capacity parameters and  $SIF_{\text{PSII}}$  (due to the regulation  
566 of  $q_L$ ). This explains the conflicting results reported in previous studies (*e.g.*, Zhang *et al.*, 2014  
567 and Camino *et al.*, 2019 vs Fu *et al.*, 2021 and Koffi *et al.*, 2015). Indeed, from our theoretical  
568 formulation (eqn 8-9), it is mechanistically unwarranted to expect simple relationship between  
569 photosynthetic capacity parameters and SIF (or  $SIF_{\text{PSII}}$ ) across different species and/or  
570 environmental conditions even when the measurement settings used to obtain SIF and  
571 photosynthetic capacity parameters are exactly the same. It should be noted that the usage of  
572 modeled  $SIF_{\text{PSII}}$  (eqn 13) rather than directly measured leaf-level ChlF emission spectra (in  
573 absolute radiometric units, *e.g.*, Magney *et al.*, 2019; Meeker *et al.*, 2021) is not the cause of the  
574 differences among studies, as a strong correlation between  $SIF_{\text{PSII}}$  and ChlF emission spectra were  
575 already confirmed elsewhere (Han *et al.*, under review).

576 Specifically, our results appear to differ from model simulations (Zhang *et al.*, 2014;  
577 Camino *et al.*, 2019), which reported the significant positive relationships between simulated SIF

578 and  $V_{\text{cmax}25}$ . The discrepancy might be because our analysis of  $SIF_{\text{PSII}}$  and photosynthetic capacity  
579 parameters relationships were conducted for different plant species, while the existing studies  
580 focused on single crop types to infer  $V_{\text{cmax}25}$  with SIF. To mimic their settings, we pooled our  
581 measurements from the same species and performed regression analysis between  $SIF_{\text{PSII}}$  and  
582 photosynthetic capacity parameters (Fig. 8). However, the correlations between  $SIF_{\text{PSII}}$  and  $V_{\text{cmax}25}$   
583 ( $J_{\text{max}25}$ ) were still very weak ( $R^2 = 0.06$  for  $V_{\text{cmax}25}$ ;  $R^2 = 0.09$  for  $J_{\text{max}25}$ ). A major reason for this  
584 weak within-species correlation is that their relationships are affected by any instantaneous or  
585 long-term factors that affect photosynthesis. Another possible reason is that, in their studies, SIF  
586 was simulated by perturbing  $V_{\text{cmax}25}$  in SCOPE, a model that was tested only for a limited number  
587 of plant types, *i.e.*, crops or temperate young woody plants, grown in greenhouse/chambers/pots,  
588 and therefore inevitably suffers from model structure/parameters uncertainties. The derived SIF-  
589  $V_{\text{cmax}25}$  relationships could thus be inaccurate.

590 On the other hand, strong negative correlation between  $V_{\text{cmax-T}}$  and  $J_{\text{max-T}}$  fitted under  
591 measuring air temperatures with  $\Phi_{\text{SIF}}$  (instead of SIF) was observed among 10 tobacco (*Nicotiana*  
592 *tabacum*) cultivars (Fu *et al.*, 2021). Yet, our study did not find such negative relationship of either  
593  $V_{\text{cmax}} (J_{\text{max}}) \sim \Phi_{\text{SIF}}$  or  $V_{\text{cmax}25} (J_{\text{max}25}) \sim \Phi_{\text{SIF}}$  across a wide range of species from different PFTs.  
594 Such discrepancy is likely because Fu *et al.* (2021) confined their analyses to narrowed  
595 environmental conditions (*e.g.*, midday only, stratified to different phenological stages) and to a  
596 single plant species. In addition, they analyzed the leaf-level  $V_{\text{cmax-T}}$  and  $J_{\text{max-T}}$  with  $\Phi_{\text{SIF}}$  derived  
597 from canopy-level measurements of SIF; therefore, the scaling mismatch between leaf and canopy  
598 might also have contributed to the observed discrepancies.

599 Note that this study focuses on the leaf level. Even at the leaf scale the relationship between  
 600  $SIF_{PSII}$  and photosynthetic capacity parameters is already complex. At the canopy scale, there are  
 601 additional complexities, *i.e.*, canopy geometry/structure, re-absorption of SIF within the canopy,  
 602 vertical variations of  $q_L$ , that can further affect the strength (and potentially even the sign) of  
 603 remotely sensed SIF -  $V_{cmax}$  ( $J_{max}$ ) relationships. More measurements at the canopy scale across  
 604 broad environmental conditions and larger variety of plant species are critically needed in the  
 605 future.

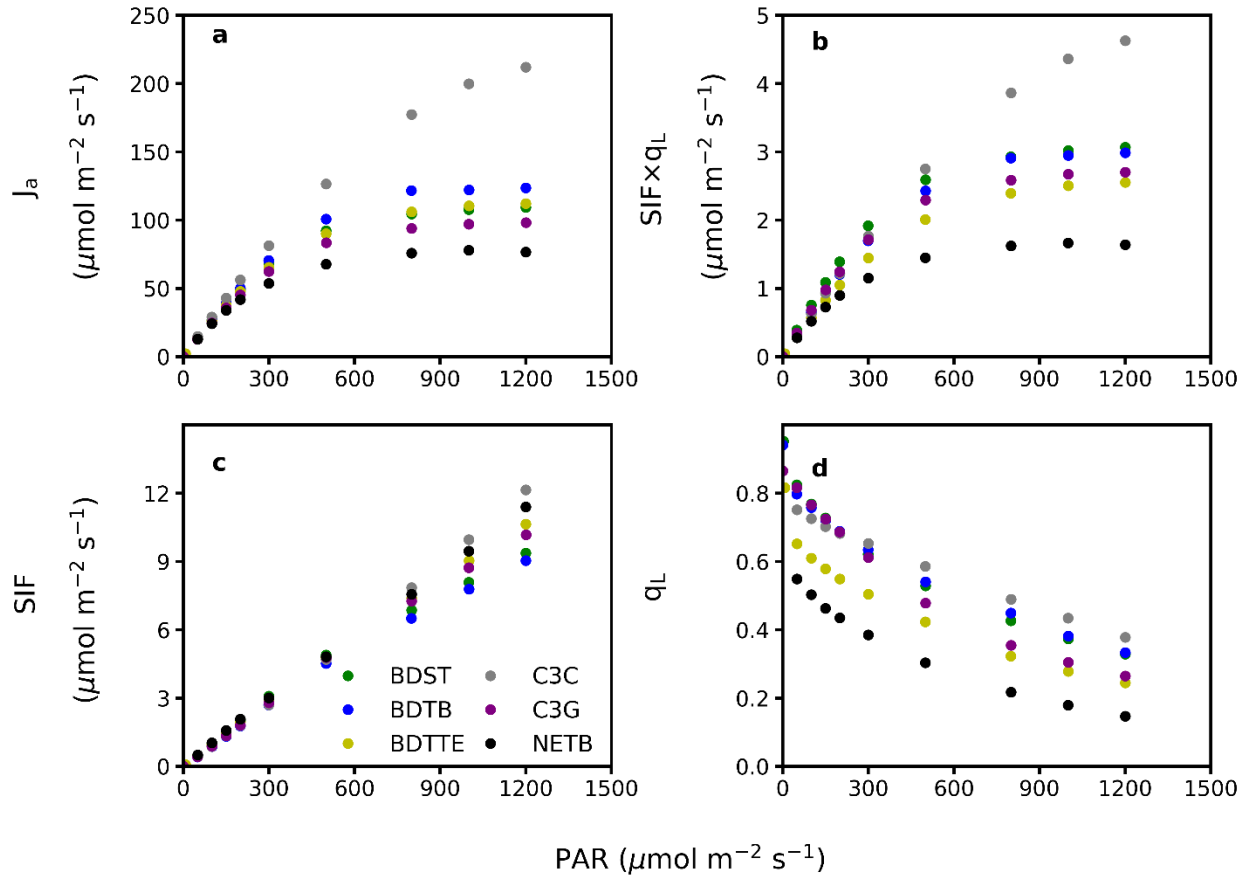


606  
 607 **Fig. 8.** Similar to Fig. 3, but the data were grouped into different species (LITU: green, QUSH:  
 608 blue, QUFA: yellow)

609

610 **Inferring photosynthetic capacity parameters with  $SIF_{PSII}$  must consider the photosynthetic**  
611 **limiting stages**

612 We observed different regression slopes of  $V_{cmax25}$  and  $SIF_{PSII} \times q_L$  between Rubisco and RuBP-  
613 regeneration limitations, which is theoretically supported by eqn 8 and eqn 9. This suggests that  
614 when SIF (or  $SIF_{PSII}$ ) is used to infer  $V_{cmax25}$ , we need *a priori* information of which photosynthetic  
615 limitation the observed SIF (or  $SIF_{PSII}$ ) is under. The determination of carboxylation limitation  
616 state depends on  $CO_2$  level, temperature, PAR, and other environment conditions. To utilize SIF  
617 (or  $SIF_{PSII}$ )  $\times q_L$  for accurately inferring  $V_{cmax25}$  and  $J_{max25}$  beyond the leaf level, we need to first  
618 determine the carboxylation limitation state with ChlF information itself. Sharkey *et al.* (2007)  
619 reported that ChlF measurements can be used to determine the limiting stages for any data point  
620 by analyzing the response of  $J_a$  to  $CO_2$  concentration. Similarly, the response of  $J_a$  to PAR can be  
621 also used to identify the limiting stages. For example, if  $J_a$  is increasing with PAR, the data belong  
622 to the RuBP-regeneration limitation. If  $J_a$  reaches a plateau with PAR, the data are Rubisco-limited.  
623 Interestingly, we observed similar patterns between  $J_a$  and  $SIF_{PSII} \times q_L$  with PAR (Fig. 9), which  
624 indicated that the response of  $SIF_{PSII} \times q_L$  to environmental factor would be useful to identify the  
625 carboxylation limitation states. The consistent trends of  $J_a$  and  $SIF_{PSII} \times q_L$  can be also explained by  
626 the equation of  $J_a$  (eqn 1).



627  
 628 **Fig. 9.** The response of  $J_a$  (a),  $SIF_{PSII} \times q_L$  (b),  $SIF_{PSII}$  (c), and  $q_L$  (d) on PAR at different PFTs.

629 Different colors represent different PFTs. Each scatter represents the mean of all species within  
 630 the same PFT.

631

632

633 **Conclusion**

634 This study revealed that  $SIF_{PSII}$  alone is incapable of informing the variations in  $V_{cmax25}$  and  $J_{max25}$   
635 either within a species or across different species, even when  $SIF_{PSII}$  is determined under the same  
636 environmental conditions. In contrast, the product of  $SIF_{PSII}$  and the fraction of open PSII reaction  
637 centers  $q_L$ , which indicates the redox state of PSII, is a strong predictor of both  $V_{cmax25}$  and  $J_{max25}$ .  
638 The limitation state of carboxylation must be considered if observed  $SIF_{PSII}$  is utilized to infer  
639  $V_{cmax25}$  (or  $J_{max25}$ ) under dynamic environmental conditions. Temperature variations can further  
640 complicate the relationships of photosynthetic capacity parameters with  $SIF_{PSII} \times q_L$ , but such  
641 relationships remain relatively stable if considered at the same temperatures. These findings are  
642 grounded on the consistency between theoretical reasoning and direct measurements on a diverse  
643 number of species and expected to have high rigor and robustness.

644

645

646 **Acknowledgments**

647 This study is supported by NSF Macrosystem Biology (Award 1926488). JH, JW, and YS also  
648 acknowledge support from USDA-NIFA Hatch Fund (1014740). ORNL is managed by UT-  
649 Battelle, LLC, for DOE under contract DE-AC05-00OR22725.

650 **Conflict of Interest**

651 The authors declare that there is no conflict of interest.

652 **Author contributions**

653 JH and YS planned and designed the research. JH performed experiments and analyzed data. JH,  
654 LG and YS wrote the manuscript. JW performed the statistical analysis.

655 **Data Availability**

656 Data available on request from the authors.

657 **Supplementary data**

658 **Notes S1.** The full derivations of the theoretical equations linking photosynthetic capacity  
659 parameters with  $SIF_{PSII}$  (Eqn 5-6)

660 **Notes S2.** Validity of the theoretical equations (Eqn 5-6) in directly computing photosynthetic  
661 capacity parameters

662 **Fig. S1.** The relationships between the theoretical  $V_{cmax}$  from eqn 5 and that derived from the  
663 standard approach across different PFTs (a, for  $V_{cmax25}$ ) and across temperatures for a subset of  
664 plant species for which measurements under different temperatures are available (b, for  $V_{cmax-T}$ ,  
665 circle: LITU, triangle: QUSH, square: QUFA) under the Rubisco-limited states.

666 **Running head:** the role of  $q_L$  in inferring  $V_{cmax}$  using  $SIF_{PSII}$

667 **Reference**

668 **Arrhenius S. 1915.** Quantitative Laws in Biological Chemistry, Bell: London.

669 **Bailey-Serres J, Parker JE, Ainsworth EA, Oldroyd GED, Schroeder J. 2019.** Genetic  
670 strategies for improving crop yields. *Nature* **575**: 109–118.

671 **Bernacchi CJ, Singaas EL, Pimentel C, Portis JR AR, Long SP. 2001.** Improved temperature  
672 response functions for models of Rubisco-limited photosynthesis. *Plant Cell and*  
673 *Environment* **24**: 253–259.

674 **Björkman O, Demmig B. 1987.** Photon yield of O<sub>2</sub> evolution and chlorophyll fluorescence  
675 characteristics at 77 K among vascular plants of diverse origins. *Planta* **170**: 489–504.

676 **Bonan GB, Lawrence PJ, Oleson KW, Levis S, Jung M, Reichstein M, Lawrence DM,**  
677 **Swenson SC. 2011.** Improving canopy processes in the Community Land Model version  
678 4(CLM4) using global flux fields empirically inferred from FLUXNET data, *Journal of*  
679 *Geophysical Research* **116**: G02014.

680 **Busch FA. 2014.** Opinion: the red-light response of stomatal movement is sensed by the redox  
681 state of the photosynthetic electron transport chain. *Photosynthetic Research* **119**: 131–140.

682 **Camino C, Gonzalez-Dugo V, Hernandez P, Zarco-Tejada PJ. 2019.** Radiative transfer  $V_{\text{cmax}}$   
683 estimation from hyperspectral imagery and SIF retrievals to assess photosynthetic  
684 performance in rainfed and irrigated plant phenotyping trials. *Remote Sensing of Environment*  
685 **231**: 111186.

686 **Cooper GM. 2000.** The Chloroplast Genome. The Cell: A Molecular Approach (2nd ed.).  
687 Washington, DC: ASM Press. ISBN 978-0-87893-106-4.

688 **Croft H, Chen JM, Luo X, Bartlett P, Chen B, Staebler RM. 2017.** Leaf chlorophyll content as  
689 a proxy for leaf photosynthetic capacity. *Global Change Biology* **23**: 3513–3524.

690 **Demmig-Adams B, Garab G, Adams III W, Govindjee, Eds. 2014.** “Non-Photochemical  
691 Quenching and Energy Dissipation” in *Plants, Algae and Cyanobacteria* (Springer, Dordrecht).

692 **Detto M, Xu X. 2020.** Optimal leaf life strategies determine  $V_{\text{max}}$  dynamic during ontogeny. *New*  
693 *Phytologist* **228**: 361–375.

694 **Farquhar GD, von Caemmerer S, Berry JA. 1980.** A biochemical model of photosynthetic CO<sub>2</sub>  
695 assimilation in leaves of C3 species. *Planta* **149**: 78–90.

696 **Field C, Mooney HA. 1986.** The photosynthesis-nitrogen relationship in wild plants. In: Givnish  
697 T, eds. *On the Economy of Plant Form and Function*. Cambridge University Press, 25–55.

698 **Foyer CH, Neukermans J, Queval G, Noctor G, Harbinson J. 2012.** Photosynthetic control of  
699 electron transport and the regulation of gene expression. *Journal of Experimental Botany* **63**:  
700 1637–1661.

701 **Frankenberg C, Fisher JB, Worden J. 2011.** New global observations of the terrestrial carbon  
702 cycle from GOSAT: Patterns of plant fluorescence with gross primary productivity.  
703 *Geophysical Research Letters*. **38**: L17706.

704 **Fu P, Meacham-Hensold K, Siebers MH, Bernacchi CJ. 2021.** The inverse relationship between  
705 solar-induced fluorescence yield and photosynthetic capacity: benefits for field phenotyping.  
706 *Journal of Experimental Botany* **72**: 1295–1306.

707 **Fu P, Meacham-Hensold K, Guan K, Bernacchi CJ. 2019.** Hyperspectral leaf reflectance as  
708 proxy for photosynthetic capacities: an ensemble approach based on multiple machine  
709 learning algorithms. *Frontiers in Plant Science* **10**: 730.

710 **Genty B, Briantais J-M, Baker NR. 1989.** The relationship between the quantum yield of  
711 photosynthetic electron transport and quenching of chlorophyll fluorescence. *Biochimica et*  
712 *Biophysica Acta* **990**: 87–92.

713 **Glowacka K, Kromdijk J, Kucera K, Xie J, Cavanagh AP, Leonelli L, Leakey ADB, Ort DR,**  
714 **Niyogi KK, Long SP. 2018.** Photosystem II Subunit S overexpression increases the  
715 efficiency of water use in a field-grown crop. *Nature Communication* **9**: 868.

716 **Gu LH, Han JM, Wood JW, Sun Y. 2019.** Sun-induced Chl fluorescence and its importance for  
717 biophysical modeling of photosynthesis based on light reactions. *New Phytologist* **223**: 1179–  
718 1191.

719 **Gu LH, Pallardy SG, Tu K, Law BE, Wullschleger SD. 2010.** Reliable estimation of  
720 biochemical parameters from C3 leaf photosynthesis-intercellular carbon dioxide response  
721 curves. *Plant Cell Environment* **33**: 1852–1874.

722 **Guanter L, Frankenberg C, Dudhia A, Lewis PE, Gómez-Dans J, Kuze A, Suto H, Grainger**  
723 **RG. 2012.** Retrieval and global assessment of terrestrial chlorophyll fluorescence from  
724 GOSAT space measurements. *Remote Sensing of Environment* **121**: 236–251.

725 **Johnson F, Eyring H, Williams R. 1942.** The nature of enzyme inhibitions in bacterial  
726 luminescence: sulphanilamide, urethane, temperature, pressure. *Journal of Cell Comparative*  
727 *Physiology* **20**: 247–268.

728 **Johnson JE, Berry JA. 2021.** The role of Cytochrome  $b_6/f$  in the control of steady-state  
729 photosynthesis: a conceptual and quantitative model. *Photosynthesis Research* **148**: 101–136.

730 **Joiner J, Guanter L, Lindstrot R, Voigt M, Vasilkov AP, Middleton EM, Huemmrich KF,**  
731 **Yoshida Y, Frankenberg C. 2013.** Global monitoring of terrestrial chlorophyll fluorescence  
732 from moderate spectral resolution near-infrared satellite measurements: Methodology,  
733 simulations, and application to GOME-2. *Atmospheric Measurement Techniques* **6**: 2803–  
734 2823.

735 **Joliot P, Johnson GN. 2011.** Regulation of cyclic and linear electron flow in higher plants. *Proc*  
736 *Natl Acad Sci USA* **108**: 13317–13322.

737 **Kattge J, Bönisch G, Díaz S, Lavorel S, Prentice IC, Leadley P, Tautenhahn S, Werner GDA,**  
738 **Aakala T, Abedi M et al. 2020.** TRY plant trait database – enhanced coverage and open  
739 access. *Global Change Biology* **26**: 119–188.

740 **Koffi EN, Rayner PJ, Norton AJ, Frankenberg C, Scholze M. 2015.** Investigating the  
741 usefulness of satellite-derived fluorescence data in inferring gross primary productivity  
742 within the carbon cycle data assimilation system. *Biogeosciences* **12**: 4067–4084.

743 **Kramer DM, Evans JR. 2011.** The importance of energy balance in improving photosynthetic  
744 productivity. *Plant Physiology* **155**: 70–78.

745 **Kramer DM, Johnson G, Kiirats O, Edwards GE. 2004.** New fluorescence parameters for the  
746 determination of  $Q_A$  redox state and excitation energy fluxes. *Photosynthesis Research* **79**:  
747 209–218.

748 **Kromdijk J, Glowacka K, Long SP. 2019.** Predicting light-induced stomatal movements based  
749 on the redox state of plastoquinone: theory and validation. *Photosynthesis Research* **141**: 83–  
750 97.

751 **Long SP, Postl WF, Bolharnordenkampf HR. 1993.** Quantum yields for uptake of carbon  
752 dioxide in C3 vascular plants of contrasting habitats and taxonomic groupings. *Planta* **189**:  
753 226–234.

754 **Magney TS, Frankenberg C, Köhler P, North G, Davis TS, Dold C, Dutta D, Fisher JB,**  
755 **Grossmann K, Harrington A et al. 2019.** Disentangling changes in the spectral shape of  
756 chlorophyll fluorescence: Implications for remote sensing of photosynthesis. *Journal of*  
757 *Geophysical Research: Biogeosciences* **124**: 1491–1507.

758 **Meacham-Hensold K, Montes CM, Wu J, Guan K, Fu P, Ainsworth EA, Pederson T, Moore**  
759 **CE, Brown KL, Raines C, Bernacchi CJ. 2019.** High-throughput field phenotyping using  
760 hyperspectral reflectance and partial least squares regression (PLSR) reveals genetic  
761 modifications to photosynthetic capacity. *Remote Sensing of Environment* **231**: 111176.

762 **Medlyn BE, Dreyer E, Ellsworth D, Forstreuter M, Harley PC, Kirschbaum MUF, le Roux**  
763 **X, Montpied P, Strassmeyer J, Walcroft A, Wang K, Loustau D. 2002.** Temperature  
764 response of parameters of a biochemically based model of photosynthesis. II. A review of  
765 experimental data. *Plant, Cell and Environment* **25**: 1167–1179.

766 **Meeker EW, Magney TS, Bambach N, Momayyezi M, McElrone AJ. 2021.** Modification of a  
767 gas exchange system to measure active and passive chlorophyll fluorescence simultaneously  
768 under field conditions. *AoB Plants* doi:10.1093/aobpla/plaa066.

769 **Mohammed GH, Colombo R, Middleton EM. 2019.** Remote sensing of solar-induced  
770 chlorophyll fluorescence (SIF) in vegetation: 50 years of progress. *Remote Sensing of*

771 *Environment* **231**: 111177.

772 **Morison JIL, Gifford RM. 1982.** Stomatal Sensitivity to Carbon Dioxide and Humidity. A  
773 comparison of two C3 and two C4 grass species. *Plant Physiology* **71**: 789–796.

774 **Oxborough K, Baker NR. 1997.** Resolving chlorophyll a fluorescence images of photosynthetic  
775 efficiency into photochemical and non-photochemical components-calculation of qP and  
776  $F_v'/F_m'$  without measuring  $F_o'$ . *Photosynthesis Research* **54**:135–142.

777 **Papageorgiou GC, Govindjee G. 2004.** Chlorophyll Fluorescence: A Signature of Photosynthesis.  
778 Springer, Dordrecht.

779 **Porcar-Castell A, Tyystjärvi E, Atherton J, van der Tol C, Flexas J, Pfündel EE, Moreno J,**  
780 **Frankenberg C, Berry JA. 2014.** Linking chlorophyll a fluorescence to photosynthesis for  
781 remote sensing applications: mechanisms and challenges. *Journal of Experimental Botany* **65**:  
782 4065–4095.

783 **Pospisil P, Skotnica J, Naus J. 1998.** Low and high temperature dependence of minimum  $F_o$  and  
784 maximum  $F_M$  chlorophyll fluorescence in vivo. *Biochimica et Biophysica Acta* **1363**: 95–99.

785 **Roach T, Krieger-Liszkay A. 2014.** Regulation of photosynthetic electron transport and  
786 photoinhibition. *Current Protein and Peptide Science* **15**: 351–362.

787 **Rochaix JD. 2011.** Regulation of photosynthetic electron transport. *Biochimica et Biophysica Acta*  
788 *- Bioenergetics* **1807**: 375–383.

789 **Rogers A, Medlyn BE, Dukes JS, Bonan G, von Caemmerer S, Dietze MC, Kattge J, Leakey**  
790 **ADB, Mercado LM, Niinemets Ü et al. 2017.** A roadmap for improving the representation  
791 of photosynthesis in Earth system models. *New Phytologist* **213**: 22–42.

792 **Schaefer K, Schwalm CR, Williams C, Arain MA, Barr A, Chen JM, Davis KJ, Dimitrov D,**  
793 **Hilton TW, Hollinger DY et al. 2012.** A model-data comparison of gross primary  
794 productivity: Results from the North American Carbon Program site synthesis. *Journal of*  
795 *Geophysical Research: Biogeosciences* **117**: G03010.

796 **Schreiber U. 2004.** Pulse-Amplitude-Modulation (PAM) Fluorometry and Saturation Pulse  
797 Method: An Overview. In: Papageorgiou G.C., Govindjee (eds) Chlorophyll a Fluorescence.  
798 Advances in Photosynthesis and Respiration, Springer, Dordrecht, **19**: 279–319.

799 **Serbin SP, Singh A, Desai AR, Dubois SG, Jablonski AD, Kingdon CC, Kruger EL,**  
800 **Townsend PA. 2015.** Remotely estimating photosynthetic capacity, and its response to  
801 temperature, in vegetation canopies using imaging spectroscopy. *Remote Sensing of*  
802 *Environment* **167**: 78–87.

803 **Sharkey TD, Bernacchi CJ, Farquhar GD, Singaas EL. 2007.** Fitting photosynthetic carbon  
804 dioxide response curves for C3 leaves. *Plant, Cell, and Environment* **30**: 1035–1040.

805 **Sharkey TD. 1985.** O<sub>2</sub>-insensitive photosynthesis in C3 plants: its occurrence and a possible  
806 explanation. *Plant Physiology* **78**: 71–75.

807 **Simkin AJ, López-Calcagno PE, Raines CA. 2019.** Feeding the world: improving  
808 photosynthetic efficiency for sustainable crop production. *Journal of Experimental Botany*  
809 **70**: 1119–1140.

810 **Simkin AJ, McAusland L, Headland LR, Lawson T, Raines CA. 2015.** Multigene manipulation  
811 of photosynthetic carbon assimilation increases CO<sub>2</sub> fixation and biomass yield in tobacco.  
812 *Journal of Experimental Botany* **66**: 4075–4090.

813 **South PF, Cavanagh AP, Liu HW, Ort DR. 2019.** Synthetic glycolate metabolism pathways  
814 stimulate crop growth and productivity in the field. *Science* **363(6422):** eaat9077.

815 **Stinziano JR, Roback C, Gamble D, Murphy B, Hudson P, Muir CD. 2020.** Photosynthesis:  
816 tools for plant ecophysiology & modeling. R package version 2.0.1.

817 **Tesa M, Thomson S, Gakamsky A. 2018.** Temperature-dependent quantum yield of fluorescence  
818 from plant leaves. *Application notes in Edinburgh instruments.* AN\_P41.

819 **Vilfan N, van der Tol C, Verhoef W. 2019.** Estimating photosynthetic capacity from leaf  
820 reflectance and Chl fluorescence by coupling radiative transfer to a model for photosynthesis.  
821 *New Phytologist* **223:** 487–500.

822 **van der Tol C, Berry JA, Campbell PKE. 2014.** Models of fluorescence and photosynthesis for  
823 interpreting measurements of solar-induced chlorophyll fluorescence. *Journal of Geophysical*  
824 *Research: Biogeosciences* **119:** 2312–2327.

825 **van der Tol C, Verhoef W, Timmermans J, Verhoef A, Su Z. 2009.** An integrated model of  
826 soil-canopy spectral radiances, photosynthesis, fluorescence, temperature and energy  
827 balance. *Biogeosciences* **6:** 3109–3129.

828 **von Caemmerer S, Farquhar GD. 1981.** Some relationships between the biochemistry of  
829 photosynthesis and the gas exchange of leaves. *Planta* **153:** 376–387.

830 **von Caemmerer S. 2000.** Biochemical Models of Leaf Photosynthesis. Techniques in Plant  
831 Science, No. 2. CSIRO Publishing, Collingwood.

832 **Walker AP, Beckerman AP, Gu L, Kattge J, Cernusak LA, Domingues TF, Scales JC,**

833 **Wohlfahrt G, Wullschleger SD, Woodward FI. 2014.** The relationship of leaf  
834 photosynthetic traits –  $V_{\text{max}}$  and  $J_{\text{max}}$  – to leaf nitrogen, leaf phosphorus, and specific leaf  
835 area: a meta-analysis and modeling study. *Ecology and Evolution* **4**: 3218–3235.

836 **Wright IJ, Reich PB, Westoby M, Ackerly DD, Baruch Z, Bongers F, Cavender-Bares J,**  
837 **Chapin FS, Cornelissen JHC, Diemer M et al. 2004.** The world-wide leaf economics  
838 spectrum. *Nature* **428**: 821–827.

839 **Wullschleger SD. 1993.** Biochemical limitations to carbon assimilation in C3 plants - a  
840 retrospective analysis of the A/Ci curves from 109 species. *Journal of Experimental Botany*  
841 **44**: 907–920.

842 **Xu L, and Baldocchi DD. 2003.** Seasonal trend of photosynthetic parameters and stomatal  
843 conductance of blue oak (*Quercus douglasii*) under prolonged summerdrought and high  
844 temperature. *Tree Physiology* **23**: 865–877.

845 **Yendrek CR, Tomaz T, Montes CM, Cao Y, Morse AM, Brown PJ, McIntyre LM, Leakey**  
846 **ADB, Ainsworth EA. 2017.** High-Throughput Phenotyping of Maize Leaf Physiological and  
847 Biochemical Traits Using Hyperspectral Reflectance. *Plant Physiology* **173**: 614–626.

848 **Yin X, Busch FA, Struik PC, Sharkey TD. 2021.** Evolution of a biochemical model of steady-  
849 state photosynthesis. *Plant, cell and environment*. <https://doi.org/10.1111/pce.14070>.

850 **Yoshikawa M. 2013.** Handbook of Biologically Active Peptides (Second Edition). 1570–1576.

851 **Zhang Y, Guanter L, Joiner J, Song L, Guan K. 2018.** Spatially-explicit monitoring of crop  
852 photosynthetic capacity through the use of spacebased chlorophyll fluorescence data. *Remote*  
853 *Sensing of Environment* **210**: 362–374.

854 **Zhang YG, Guanter L., Berry JA, Joiner J., van der T, Huete A, Gitelson A, Voigt M, Kohler**  
855 **P. 2014.** Estimation of vegetation photosynthetic capacity from space-based measurements  
856 of chlorophyll fluorescence for terrestrial biosphere models. *Global Change Biology* **20:**  
857 3727–3742.

858

859 **Inference of photosynthetic capacity parameters from Chlorophyll a Fluorescence is**  
860 **affected by the redox state of PSII reaction centers**

861 Running title: The role of  $q_L$  in inferring  $V_{\text{cmax}}$  using  $SIF_{\text{PSII}}$

862 Jimei Han<sup>1\*</sup>, Lianhong Gu<sup>2</sup>, Jiaming Wen<sup>1</sup>, Ying Sun<sup>1\*</sup>

863 <sup>1</sup>School of Integrative Plant Science, Soil and Crop Science Section, Cornell University, Ithaca,  
864 NY, USA

865 <sup>2</sup>Environmental Sciences Division and Climate Change Science Institute, Oak Ridge National  
866 Laboratory, Oak Ridge, Tennessee, USA

867 \*Corresponding to: [jh2757@cornell.edu](mailto:jh2757@cornell.edu) (J. Han), [ys776@cornell.edu](mailto:ys776@cornell.edu) (Y. Sun)

868

869 **Notes S1. The full derivations of the theoretical equations linking photosynthetic capacity**  
 870 **parameters with  $SIF_{PSII}$  (Eqn 5-6)**

871 By equating the light reaction-based (MLR-SIF, eqn 1) and carbon reaction-based  $J_a$  (FvCB, eqn  
 872 2-3), we can derive explicit relationships between  $SIF_{PSII}$  and  $V_{cmax}$  (and  $J_{max}$ ). Specifically,  
 873 under the Rubisco-limited state, set  $A_g = A_c$ ; then combining eqn 2 and 3b leads to:

$$874 \frac{V_{cmax} \cdot (C_i - \Gamma^*)}{C_i + K_{CO}} = \frac{(C_i - \Gamma^*)}{4C_i + 8\Gamma^*} \times J_a. \quad (\text{eqn 4 in the main$$

875 text)

876 Inserting eqn 1 to eqn 4 results in:

$$877 \frac{V_{cmax} \cdot (C_i - \Gamma^*)}{C_i + K_{CO}} = \frac{(C_i - \Gamma^*)}{4C_i + 8\Gamma^*} \times \frac{\Phi_{PSII_{max}} \cdot (1 + k_{DF})}{1 - \Phi_{PSII_{max}}} \times q_L \times SIF_{PSII}. \quad (S1)$$

878 Thus,

$$879 V_{cmax} = \frac{C_i + K_{CO}}{(4C_i + 8\Gamma^*)} \times \frac{\Phi_{PSII_{max}}}{1 - \Phi_{PSII_{max}}} \times (1 + k_{DF}) \times q_L \times SIF_{PSII}. \quad (\text{eqn 5 in the main text})$$

880 Within the FvCB framework, the potential electron transport rate  $J_p$  is empirically calculated by:

$$881 J_p = \frac{\sigma \cdot PAR + J_{max} - \sqrt{(\sigma \cdot PAR + J_{max})^2 - 4\theta \cdot \sigma \cdot PAR \cdot J_{max}}}{2\theta}. \quad (\text{eqn 3d in the main$$

882 text)

883 Eqn S3d is a root of the following quadratic equation:

$$884 \theta \cdot J_p^2 - (\sigma \cdot PAR + J_{max})J_p + J_{max} \cdot \sigma \cdot PAR = 0. \quad (S2)$$

885 Or equivalently,

$$886 J_p = \frac{J_{max} - J_p}{J_{max} - \theta \cdot J_p} \cdot \sigma \cdot PAR. \quad (S3)$$

887 Eqn S3 shows that the FvCB model for potential electron transport is a recursive model.

888 Under the RuBP regeneration limited state, the potential electron transport rate becomes the  
 889 actual rate, *i.e.*,  $J_p = J_a$ . Solve eqn S3 for  $J_{max}$ :

$$890 \quad J_{max} = \frac{\theta \cdot J_a - \sigma \cdot PAR}{J_a - \sigma \cdot PAR} J_a.$$

891 (S4)

892 Insert eqn 3d into S4:

$$893 \quad J_{max} = \frac{\theta \cdot \frac{q_L \cdot SIF_{PSII} \cdot (1 + k_{DF})}{\sigma \cdot PAR} - \frac{1 - \Phi_{PSII_{max}}}{\Phi_{PSII_{max}}}}{\left( \frac{q_L \cdot SIF_{PSII} \cdot (1 + k_{DF})}{\sigma \cdot PAR} - \frac{1 - \Phi_{PSII_{max}}}{\Phi_{PSII_{max}}} \right)} \times \frac{\Phi_{PSII_{max}}}{1 - \Phi_{PSII_{max}}} \times (1 + k_{DF}) \times q_L \times SIF_{PSII}$$

894 (eqn 6 in the main text)

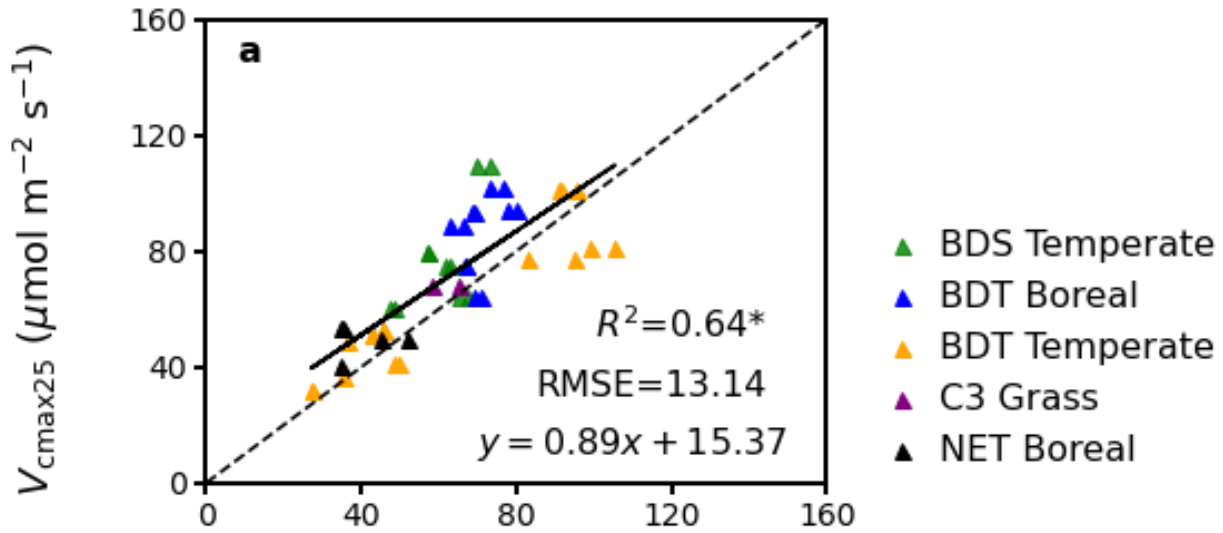
895

896 **Notes S2. Validity of the theoretical equations (Eqn 5-6) in directly computing photosynthetic**  
 897 **capacity parameters**

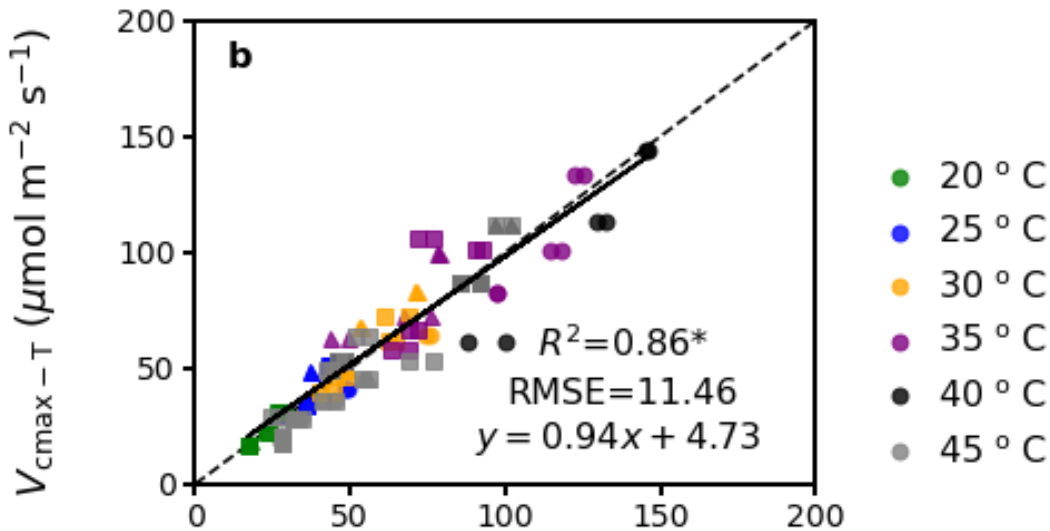
898 To demonstrate the validity of our theoretical formulations in directly deriving photosynthetic  
 899 capacity parameters, we compared  $V_{cmax}$  computed from eqn 5 (using  $V_{cmax}$  only here as an example  
 900 for illustrative purpose) by assuming the unknown parameters as constants, against that determined  
 901 from the standard approach, *i.e.*, fitting CO<sub>2</sub> and light response curves based upon the FvCB model  
 902 using the *photosynthesis* R package (Stinziano *et al.*, 2020) (details in the main text). Specifically,  
 903 to compute  $V_{cmax}$  with eqn 5, we assumed  $k_{DF}$  to be 10 for all the PFT species under different  
 904 temperatures (20, 25, 30, 35, 40, and 45 °C).  $\Gamma^*$  and  $K_{co}$  were assumed to be constant at 42.75  
 905  $\mu\text{mol mol}^{-1}$  and 435.44  $\mu\text{mol mol}^{-1}$ , respectively at 25 °C (Bernacchi *et al.*, 2001) and constant  
 906 across plant species. The temperature response function from Bernacchi *et al.* (2001) was adopted  
 907 to calibrate  $\Gamma^*$  and  $K_{co}$  at other temperatures. Then, the derived  $q_L$ ,  $SIF_{PSII}$ , and  $\Phi_{PSII_{max}}$  using PAM  
 908 parameters and directly measured  $C_i$  at saturating light (1000 and 1200  $\mu\text{mol m}^{-2} \text{s}^{-1}$ ) and ambient  
 909 CO<sub>2</sub> conditions (400  $\mu\text{mol mol}^{-1}$ ) under Rubisco-limited states were used to compute  $V_{cmax}$  with  
 910 eqn 5 under different temperatures across different plant species.

911 We observed that the  $V_{cmax}$  theoretically derived from eqn 5 was strongly correlated with  
 912 that determined from the standard approach (Fig. S1). Specifically, for  $V_{cmax25}$ , their R<sup>2</sup> is 0.64

913 with a regression slope of 0.89 ( $p < 0.05$ ) across PFTs (Fig. S1); for  $V_{\text{cmax-T}}$  their  $R^2$  is 0.86 with a  
914 regression slope of 0.94 ( $p < 0.05$ ) across temperatures for a subset of species (for which  
915 measurements under different temperatures are available, *i.e.*, LITU, QUSH, and QUFA). This  
916 result demonstrates the validity of our theoretical formulation that computes photosynthetic  
917 parameters with  $SIF_{\text{PSII}}$ . Notably, the regression slope in Fig. S1a, to some degree, deviates from  
918 the 1:1 line, which is likely a consequence of the assumed constant values for  $I^*$  and  $K_{\text{co}}$  across  
919 PFTs. This indicates that the use of assumed constants for unknown parameters can contribute to  
920 the uncertainty of our theoretical formulation for practical applications. In addition, mesophyll  
921 conductance was assumed to be infinite for  $V_{\text{cmax}}$  derived from both approaches here, which could  
922 result in the underestimation of  $V_{\text{cmax}}$  and  $J_{\text{max}}$  (Sun *et al.*, 2014). Therefore, broad applications of  
923 our theoretical formulations would require a coupling with mesophyll conductance model in the  
924 future.



Theoretical  $V_{\text{cmax}25}$  from eqn5 ( $\mu\text{mol m}^{-2} \text{s}^{-1}$ )



Theoretical  $V_{\text{cmax}-T}$  from eqn5 ( $\mu\text{mol m}^{-2} \text{s}^{-1}$ )

925

926 **Fig. S1. The relationships between the theoretical  $V_{\text{cmax}}$  from eqn 5 and that derived from the**  
 927 **standard approach across different PFTs (a, for  $V_{\text{cmax}25}$ ) and across temperatures for a subset**  
 928 **of plant species for which measurements under different temperatures are available (b, for**  
 929  **$V_{\text{cmax}-T}$ , circle: LITU, triangle: QUSH, square: QUFA) under the Rubisco-limited states. The**  
 930 **black lines are linear ordinary least-square regression with all data pooled together. \* denotes**  
 931 **statistically significant at the level of 0.05. Each scatter represents one single leaf replicate. The**

932 theoretical  $V_{\text{cmax}}$  from eqn 5 was calculated under the PAR of 1200 and 1000  $\mu\text{mol m}^{-2} \text{s}^{-1}$  and  
933 ambient  $\text{CO}_2$  conditions ( $400 \mu\text{mol mol}^{-1}$ ) at 25 °C for (a) and different temperatures (20, 25, 30,  
934 35, 40, 45 °C) for (b). The data size for each species or temperature depends on how many data  
935 samples were Rubisco-limited.

936